Weak Lesion Feature Extraction by Dual-branch Separation and Enhancement Network for Safe Hemorrhagic Transformation Prediction

Ziqiao Wang[a], Zhi Liu[a,*], Shuo Li[b]

[a]*School of Information Science and Engineering, Shandong University, Qingdao, 266237, China*

[b]*Digital Imaging Group of London, Western University, London, ON N6A 3K7, Canada*

Abstract

Hemorrhagic transformation (HT) is regarded as a safety endpoint of arterial ischemic stroke acute treatment and secondary prevention trials(Hutchinson and Beslow, 2019). Accurate HT prediction dramatically reduces the death rate from misdiagnosis. At present, HT predictions almost all rely on contrast images with perfusion agents, which is time-consuming and labor-intensive, causing secondary brain damage and high cost. Almost all machine learning algorithms cannot use non-contrast CT for HT prediction because of huge challenges. In this study, a Dual-branch Separation and Enhancement Network (DBSE-Net) is proposed for weak feature extraction and safe HT prediction without perfusion agents. DBSE-Net innovatively uses a dual-branch separation and fusion mechanism to achieve weak feature adaptive extraction. In the DBSE-Net's encoder submodules, Brain Compression Assessment Branch (BCAB) and Infarct Assessment Branch (IAB) are proposed to apply lightweight encoding structures with different receptive fields, which are adapted to the lesion area's characteristics. With the help of DBSE-Net's keyframe selection algorithm and area guidance knowledge, DBSE-Net removes redundant information and clearly describes the severity of lesions. In summary, DBSE-Net integrates global and local features to obtain multi-scale and multi-category brain status information, enhancing the weak features of non-contrast CT and realizes accurate HT prediction. Experimental Result:

*Corresponding author

Email address: liuzhi@sdu.edu.cn (Zhi Liu)

Among all 144 intracranial stroke patients diagnosed by doctors as having no HT risk, DBSE-Net identified 73 high-risk HT patients (88 HT cases in total). The result illustrates that DBSE-Net helps doctors secondary diagnose the HT risk of intracranial stroke patients and becomes a potential tool to prevent doctors from false HT risk diagnosis.

Keywords: Hemorrhagic transformation prediction, Non-contrast CT, DBSE-Net.

1. Introduction

The accurate prediction of hemorrhagic transformation (HT) can reduce the misdiagnosis rate of doctors and improve the survival rate of patients(Sussman and Connolly Jr, 2013). Nowadays, Hemorrhagic transformation (HT) is regarded as a safety endpoint of arterial ischemic stroke acute treatment and secondary prevention trials(Hutchinson and Beslow, 2019). As a common spontaneous complication after intracranial embolism, HT is easily misdiagnosed by doctors and leads to death. From 2001 to 2011, an average of 795,000 people produced a stroke or recurrent stroke (hemorrhagic or ischemic) annually in the United States, of which 185,000 people were recurrent stroke episodes(Mozaffarian et al., 2015). Doctors usually use tissue plasminogen activator (TPA) as a treatment for patients with infarction. However, if the doctor uses TPA treatment for stroke patients with high HT risk, the wrong treatment will lead to an increased HT phenomenon and even death(Larrue et al., 1997)(of Neurological Disorders and rt PA Stroke Study Group, 1995). The HT prediction method can perform an HT risk second diagnosis on stroke patients and correct the doctor's judgment. With the computer-aided HT prediction method, stroke patients with high HT risk will not use TPA treatment, which will cause secondary intracranial hemorrhage. As shown in Fig.1 (Clinical Significance), computer-aided HT prediction methods can help doctors confirm the patient's brain status and determine whether to use TPA treatment, which increases the patient's cure rate. Although there are many methods for evaluating the indicators of HT prediction, such as net water uptake (NWU)(Broocks et al., 2018)(Zhao et al., 2019), they only stop at the indicator evaluation without further systematic prediction of HT. At present, in the field of cerebrovascular accidents, there is an urgent need for an accurate, convenient, and low brain injury HT prediction method.

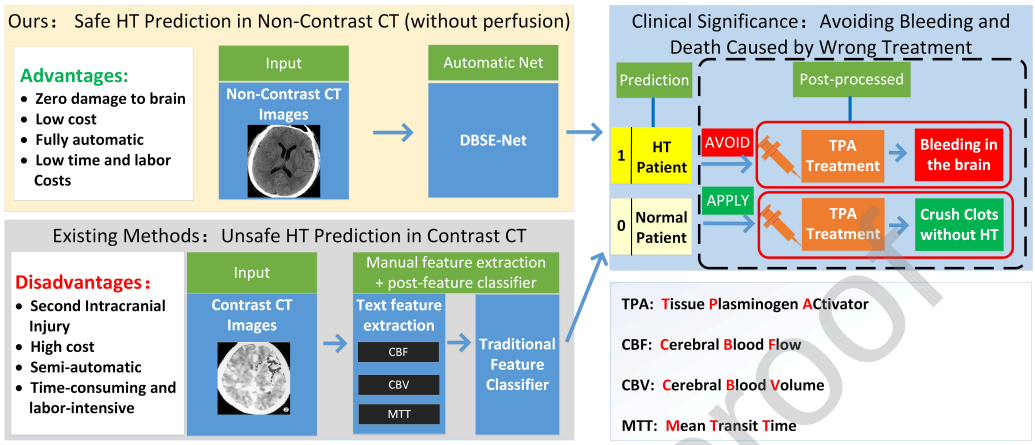

Figure 1: Significance of Predicting Hemorrhagic Transformation on Safe CT (Non-contrast)

The current HT prediction methods are based on contrast CT or contrast MRI, which have four major disadvantages (shown in Fig.1). **1)**Second Intracranial Injury: contrast CT/MRI image generation requires the injection of perfusion agents. The injected non-diffusion perfusion agents will change the relaxation time of the vascular bed in the adjacent tissue(Barbier et al., 2001), which destroys the already fragile blood vessel wall. The injection of perfusion agents eventually increases the likelihood of HT and causes other risks to patients with compromised kidney function(Xu et al., 2021). **2)**High Cost: the use of perfusion agents in CT/MRI images brings additional economic costs to patients. Contrast CT/MRI costs 1.5 times more than ordinary CT/MRI images(Wiley, 2008), making poor patients bear high economic pressure. **3)**Semi-automatic: Most existing HT prediction techniques require manual extraction of Cerebral Blood Flow (CBF), Cerebral Blood Volume (CBV), and Mean Transit Time (MTT)(Yu et al., 2019) vascular assessment features. These parameters are helpful for HT prediction but make the prediction network unable to realize fully automatic operation. **4)**Increase Time and Workload: Contrast CT also requires an additional CT scan, parameter calculation, and perfusion agent injection, which results in extra time on pathological examination. Existing Contrast CT requires continuous dynamic scanning of the region of interest (ROI) to find the perfusion agent response(Hunter et al., 1998).

Although Non-contrast CT has numerous advantages, Non-contrast CT

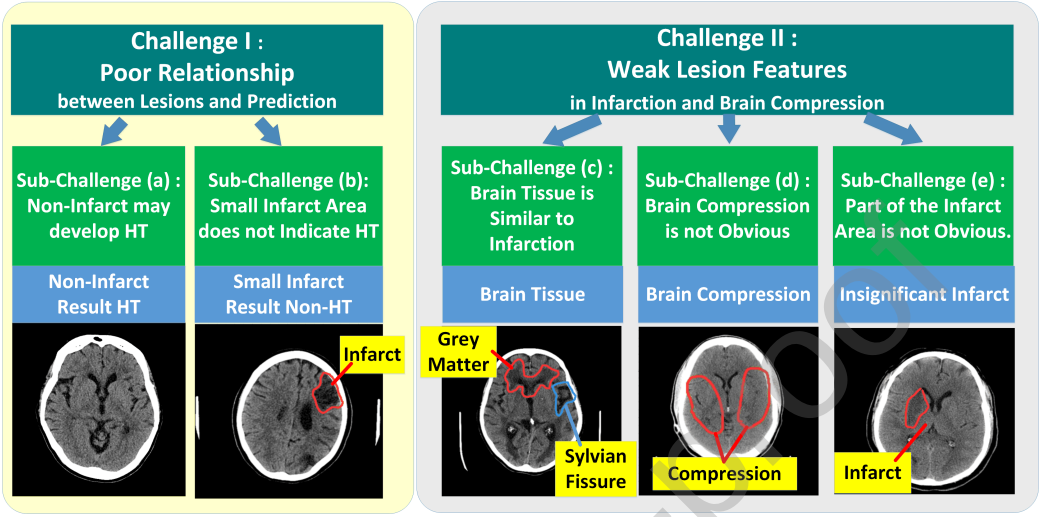

Figure 2: Challenges of safe non-contrast CT images without perfusion agent

is difficult to apply to HT prediction (Fig.2). For the non-contrast CT used for the HT prediction task, the two main challenges are as follows: **Firstly**, a poor relationship between lesion and prediction: There is no one-to-one relationship between the presence of cerebral infarction and HT in patients. In general, the larger the infarct size, the higher the possibility of HT. Nevertheless, some patients with HT do not have significant brain lesions in early diagnostic images. At the same time, patients with small infarcts in the brain do not develop HT. Like Fig. 2 (a), some patients have no obvious infarct area but develop HT results. In the Fig. 2 (b), small infarct area may not trigger HT phenomenon. **Secondary**, weak lesion features (insignificant lesions) in infarction and brain compression: Many lesions are difficult to distinguish visually, and the lesions are easily confused with brain tissue. As shown in Fig. 2 (c), the brain's inherent structure, grey matter, and sylvian are very similar to the infarct area. Not only external interference but also some lesion areas are difficult to observe, as shown in Fig. 2 (d). Brain compression manifests as an insignificant brain sulcus, but there is no clear evaluation index for insignificant sulcus. Furthermore, due to large differences in human brain structures, the infarct area is not significant for many patients. In Fig. 2 (e), the infarct area has little grey value different than the same position on the right brain region. Two major challenges indicate that HT prediction requires analysis of the brain's overall compression status and

the enhancement of local lesion features. The existing traditional neural network classification methods (ResNet(Szegedy et al., 2016), DenseNet(Huang et al., 2017), SE-Net(Hu et al., 2018)) are mainly based on the huge feature differences between semantic features. Simultaneously, traditional networks need a close relationship between image and prediction results. However, traditional networks are weak for medical image prediction tasks where semantic information is insufficient. Non-contrast CT images cannot clearly express future results is another problem for traditional neural networks.

This paper proposes a Dual-branch Separation and Enhancement Network (DBSE-Net) for HT prediction from non-contrast CT. DBSE-Net can correctly assess the deterioration of brain infarct area and brain compression, thereby achieving accurate prediction of HT. DBSE-Net is based on the principle that HT is associated with the intracranial infarct area and the brain's midline displacement status (intracranial compression status). Based on the principle, the overall framework of DBSE-Net proposes a dual-branch lesion region separation processing mechanism. DBSE-Net consists of four layers: 1) Concerning enormous useless frames of clinical CT images, the brain keyframe selection layer is proposed to extract two keyframe images from 64 non-contrast CT images based on Alberta stroke program early CT score (ASPECTS). 2) In the brain region segmentation layer, Variable Weight UNet (VW-UNet) is proposed to pre-segment brain regions and separate global and local features. VW-UNet uses an infarct-focused segmentation model to effectively pre-segment the brain region and obtain lesion guidance knowledge, solving the weak semantic feature information problem. 3) Simultaneously, the Brain Compression Assessment Branch (BCAB) and Infarct Assessment Branch (IAB) in the dual-branch feature encoding layer are introduced to encode features, accurately extracting and enhancing different forms of features. To accurately express the severity of lesions, the brain region segmentation layer extracts lesion guidance knowledge to guide BCAB's and IAB's encoding structure training. 4) Based on lesion region separation processing mechanism and fully connection prediction layer, multi-scale and multi-category weak features are extracted to achieve accurate HT prediction.

The contributions and advantages are shown as follows:

- For the first time, we achieved a non-contrast CT-based HT prediction method, which is safe, free of secondary brain injury, low cost, and less workload. The method saves the lives of intracranial stroke patients

who are misdiagnosed by doctors.

- A dual-branch feature separation and enhancement network (DBSE-Net) is proposed to model the relationship between lesions and HT prediction results. DBSE-Net enhances the relationship between images and prediction results through guiding knowledge and a dual-branch adaptive encoding mechanism (extracting multi-category and multi-scale features), and enable non-contrast CT for HT prediction.

- Our proposed algorithm structure effectively solves the weak lesion feature problem. In the interference removal aspect, DBSE-Net proposes the ASPECTS keyframe selection layer to obtain keyframe information of the lesion area, which effectively solves network overfitting. In the feature processing aspect, we propose a separating brain lesion features (VW-UNet) and adaptive encoding (BCAB and IAB) mechanism based on clinical criteria. By encoding different lesion ROI according to their characteristics, effective weak feature extracting is achieved.

2. Related Works

Our proposed DBSE-Net is the first neural network that uses non-contrast CT for HT prediction. Other scholars all use perfusion contrast CT/MRI to apply accurate HT prediction methods.

Clinical medicine field: (Knight et al., 1998) used male Wistar rats based on T1-weighted and T2-weighted MRI to prove that Gd-DTPA is a reliable predictor of HT. (Aviv et al., 2009) proved that the product map measurement of permeability surface area appears promising for HT prediction with AUC of 0.918, the sensitivity of 77%, and specificity of 94%. (Lin et al., 2007) also proved that elevated permeability by using first-pass PCT could predict subsequent HT. (Bang et al., 2007) explained the permeability images derived from pretreatment perfusion MRI source data might identify patients at risk for HT with a sensitivity result of 83% while (Yen et al., 2016) got 78.6%. (Neumann-Haefelin C. et al., 2002) pointed out that the key to HT prediction is the disturbance of the blood-brain barrier but not of other MR parameters. (Kim et al., 2005) investigation in 55 cases showed that early parenchymal enhancement is highly specific for HT. They also pointed out that early reperfusion and damage to the blood-brain barrier in ischemic tissue may also be associated with HT's appearance. Moreover, diffusion-weighted imaging lesion volumes and apparent diffusion coefficient

indexes had no strong relationship with HT. However, (C et al., 2002) also proposed: a measurement of minimum apparent diffusion coefficient (ADC) values within an acute middle cerebral artery (MCA) stroke can achieve high-risk predictions for HT. Relative cerebral blood flow, relative cerebral blood volume, and time to maximum multi-parameter prediction methods are also proposed by (Yassi Nawaf et al., 2013). Both (Broocks et al., 2018) and (Zhao et al., 2019) proposed that net water uptake (NWU) is an important indicator of the severity of lesions in the infarct area, and it is also helpful for subsequent HT prediction.

Machine learning field: In recent years, modeling analysis and machine learning are performed on HT predictions. Compared with traditional machine learning, (Yu et al., 2018)'s kernel spectral regression method has achieved the highest accuracy of 83.7±2.6%. (Wang et al., 2020) used the Lasso logistic regression prediction model to accurately predict HT on a vast dataset (621,178 patients) and obtained an AUC of 0.78. Meanwhile, (Bouts et al., 2017) adopted a generalized linear model and random forest predictive algorithms to achieve HT prediction based on MRI datasets, which achieved AUC results of 0.85±0.14 and 0.89±0.09 in the two experimental groups. (Yu et al., 2019) adopted the LSTM network based on PWI combined with DWI imaging features into a fully connected neural network and verified that its AUC-ROC of 89.4% on 155 acute stroke patients. In addition to the HT prediction method, (Qiu et al., 2020) uses the U-Net(Ronneberger et al., 2015) transfer learning in the infarct region segmentation based on non-contrast CT and integrates multiple image features into the random forest to achieve accurate segmentation of the infarct region. Although the current HT prediction accuracy rate based on contrast images has reached a satisfactory status, no one ever tried non-contrast for HT prediction.

3. Method overview

As shown in Fig.3, Dual-branch Separation and Enhancement Network (DBSE-Net) consists of four modules as shown below. The four innovative modules achieve accurate prediction of HT based on non-contrast CT by removing redundant information, the separation and fusion of features based on clinical conditions, the adaptive feature encoding structure, and the introduction of guidance knowledge.

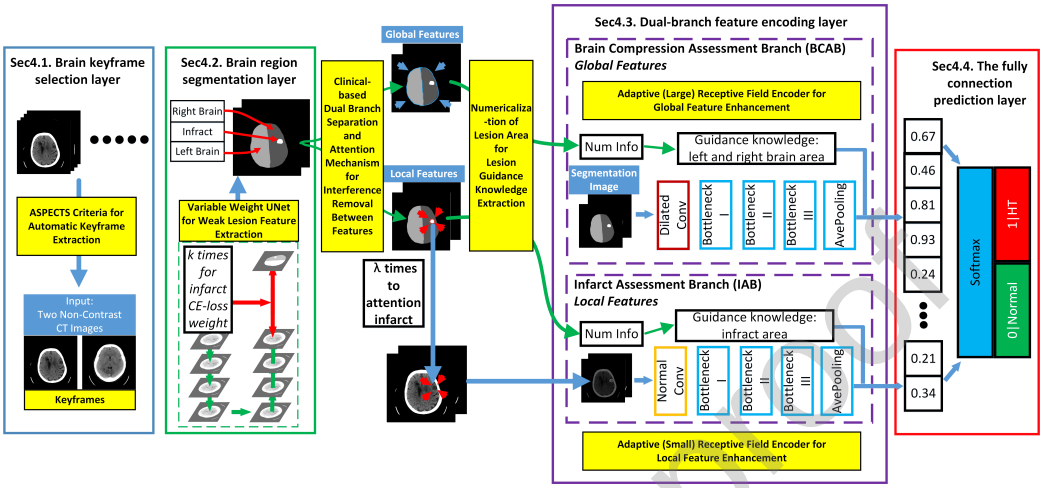

Figure 3: DBSE-Net Structure: Global and local brain feature separation for weak feature separation enhancement including: Sec4.1. brain keyframe selection layer, Sec4.2. brain region segmentation layer, Sec4.3. dual-branch feature encoding layer which consists of brain compression assessment branch (BCAB) and infarct assessment branch (IAB), Sec4.4. the fully connection prediction layer.

- **Brain keyframe selection layer enables automatic keyframe refinement.** The layer innovatively uses the Alberta stroke program early CT score (ASPECTS) medical evaluation index to extract two frames from sequence CT images. The layer selects keyframes in redundant information, reducing mutual interference between non-contrast CT images. Details are shown in sec4.1.

- **Brain region segmentation layer enables lesion area adaptive separation and guidance knowledge extraction.** The layer presegments the left brain, right brain, and infarct region to achieve the separation of the global and local image features. Simultaneously, the layer is based on variable weight training, which enhances the weak lesion features (infarct area). In the layer, the numerical guidance information extracted from the coverage lesion area assists the subsequent encoding network. By the separation of local and global features, the deterioration of the infarct area, the midline displacement, and the brain compression are revealed. Details are shown in sec4.2.

- **Dual-branch feature encoding layer enables adaptive enhancement and encoding of lesion features.** To effectively obtain the

low-dimensional information property of different scales, the module innovative performs guidance knowledge fusion, enhancement, and adaptive feature encoding of global features and local features. Details are shown in sec4.3.

- **The fully connection prediction layer for multi-feature fusion.** The module achieves HT's high-risk prediction by integrating the one-dimensional feature representations of local features, global features, guidance knowledge. Details are shown in sec4.4.

4. Methodology

4.1. Brain keyframe selection layer by ASPECTS medical evaluation index

Different from the direct input of the common 64-frame CT sequence, the brain keyframe selection layer innovatively uses the ASPECTS medical criterion as the keyframe image extraction method (Fig. 3 - Sec4.1), which keeps the brain structure status' main information content. The original 64-frame non-contrast CT images contain enormous irrelevant information without the lesion area. A large amount of irrelevant information causes the neural network to learn irrelevant information and cause serious overfitting. The layer innovatively uses the ASPECTS medical evaluation index to automatically extract two keyframes that can express all brain status. As shown in Fig. 4, the automatic extraction rules for ASPECTS images are: One at the level of the thalamus and basal ganglion (red arrow) and another adjacent to the most superior margin of the ganglionic structures (green arrow). Since the relative position of the two frames of images in the 64-frame CT sequence is roughly fixed, the two ASPECTS images can be automatically obtained from the CT sequence, which is collected from the same machine. Almost all the ASPECTS images are in fixed slices, but due to the different structure of the human brain, few images should be double checked in case there is an outlier. Neuroradiologists generally agree that the patient skull's pathological brain status can be obtained from two ASPECTS images(Pexman et al., 2001), proving the selection method is effective and in line with clinical criteria. With two keyframes, the brain lesion information of all 64-frame CT non-contrast images can be roughly obtained, avoiding the interference of enormous low-information images.

Summarized Advantages: The brain keyframe selection layer is based on ASPECTS criterion to extract two keyframes from 64 complex

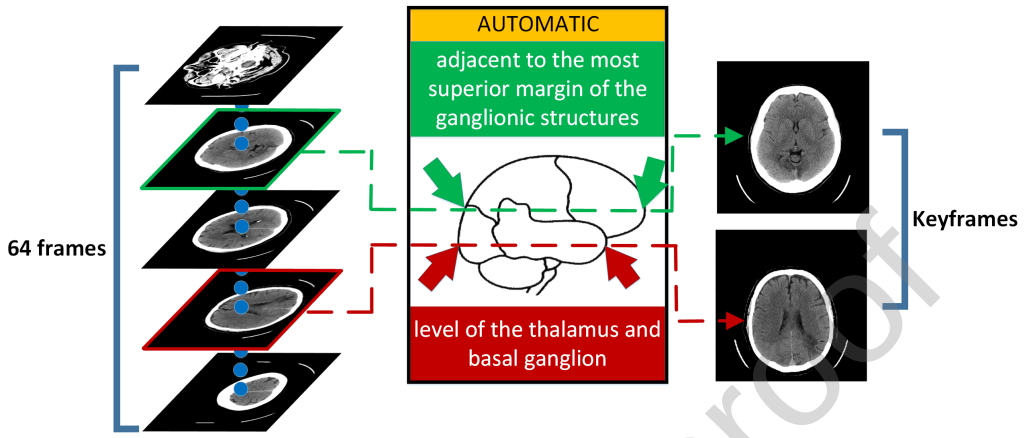

Figure 4: Schematic diagram of automatic brain keyframe selection method: CT frame extraction rules based on the Alberta stroke program early CT score.

non-contrast CT sequence images, which effectively removes redundant information according to clinicopathological characteristics.

4.2. Brain region segmentation layer by Variable Weight UNet

The brain region segmentation layer proposes Variable Weight UNet (VW-UNet) based on U-Net(Ronneberger et al., 2015) as a pre-segmentation network, which is suitable for small objects and multi-scale segmentation. The layer pre-segmentation of the three brain parts and acquisition of area guidance knowledge for the subsequent network structure (Fig. 3 - Sec4.2). From the many challenges of HT, the size of the infarct area is the core of HT prediction. Meanwhile, The characteristics of the infarct area are not significant and the midline displacement will occur between the left and right brains. Therefore, separate the infarct area from the left and right brains can accurately extract local detailed features. In VW-UNet, we input the two slices of ASPECTS images and manually label the left brain, right brain, and infarct area with a parenchymal hypoattenuation as VW-UNet training labels. Then we choose cross entropy as a loss function to train the classification results of each pixel point. Especially, to solve the infarct's weak and insignificant features, we increase the small objects (infarct) loss weight of VW-UNet by hyperparameter k times to make VW-UNet concerned about the effect of small object segmentation. In the follow-up layers, VW-UNet feeds BCAB the original segmentation image. Nevertheless, in the IAB, VW-UNet's local features weight the ASPECTS ori-images with hyperparameter λ to highlight

the infarct area importance as an attention mechanism. The formula of the attention is as follows:

$$I(i,j) = I(i,j) + \lambda * I(i,j) * S(i,j) \tag{1}$$

where I represents the IAB's input, λ represents the hyperparameter of attention mechanism. S is the brain keyframe selection layer's infarct class output (infarct segmentation image), and i, j are the pixel coordinates. Through the attention mechanism, the infarct area is highlighted so that the IAB brain local feature encoding structure focuses on the assessment of the infarct area.

Summarized Advantages: The brain region segmentation layer presegments the three brain regions through VW-UNet with a variable weight loss function, which improves the accurate segmentation of infarct regions with weak features. The layer separates the mixed global brain squeeze from the local infarct area for adaptive feature encoding. Simultaneously, the layer extracts guidance knowledge from the segmented image, solving the weak lesion features problem to a certain extent.

4.3. Dual-branch feature encoding layer by feature adaptive encoding network with different receptive fields

The dual-branch feature encoding layer obtains multi-scale and multi-category information (Fig. 3 - Sec4.3), which enriches the types of features, thereby solving the problem of weak features to a certain extent. The layer is divided into **Brain Compression Assessment Branch (BCAB)** and **Infarct Assessment Branch (IAB)**. Each branch integrates the area guidance knowledge and image features. The dual-branch separation, enhancement, and adaptive feature encoding strategy make features not interfere with each other and independently evaluate the brain status.

In BCAB, the image input is the segmentation result of the brain region segmentation layer, so as to realize the enhanced encoding of the weak brain compression feature. The receptive field of BCAB is increased to integrate the correlation between the overall structure. In the feature encoding structure, dilated convolution increases the receptive field without reducing the picture size so that BCAB subsequent structures can obtain long-ranged

information. The dilated convolution is defined as:

$$H(i,j) = \sum_{m=0}^{s-1}\sum_{n=0}^{s-1} K(m,n)G(i + \frac{(2m-s+1)\times dr}{2}, i + \frac{(2n-s+1)\times dr}{2}) \tag{2}$$

where H represents the convolution module's output, K represents the kernel of the convolution. s is expressed as the convolution kernel's size, while dr is expressed as the dilated rate. Through dilated convolution, BCAB focuses on the global structural features and brain compression state instead of local details, making BCAB assess the overall state of the brain.

In BCAB's subsequent feature encoding structure, ResNet blocks are selected to extract and generate feature maps. Average pooling is cascaded to integrate all overall brain structural features. Simultaneously, to prevent over-fitting caused by a deep layer network and numerous parameters, the ResNet block retains three layers. The area guidance knowledge is merged into the last layer of BCAB in the form of text, highlighting the midline displacement caused by the left and right brains' unequal brain area. By highlighting the brain structure, the BCAB focuses on the overall brain area's structural characteristics, selected to diagnose whether there are dangerous symptoms such as brain area deformation and blood vessel compression.

BCAB Summarized Advantages: Our newly proposed BCAB innovative provides a large-receiving field and lightweight feature encoding for global feature adaptive encoding. Through the single-dimensional feature fusion of guidance knowledge, BCAB integrates brain compression features, enhances the relationship of the weak features, and solves the phenomenon of weak features to a certain extent.

In IAB, the original ASPECTS image after attention is used as input to achieve enhanced encoding of the infarct area. A small receptive field encoder and infarct area's guidance knowledge fusion are proposed to assess the infarct areas. In general, the larger the infarct area, the higher the possibility of patients with HT after TPA. So IAB separates the local infarct for subsequent assessment of the brain infarct level is more in line with medical diagnostic criterion. In detail, IAB performs local feature encoding based on the ResNet block. Due to the small dataset, the network image encoding and dimensionality reduction ability is weak. By using transfer learning, the ImageNet pre-trained network is used for all three ResNet blocks. Like the

global branch network, the infarct area attention map also passes through a 7x7 convolutional layer with a small receptive field. With small receptive fields, IAB can get more features of the infarct area. Different from traditional ResNet, due to the insufficient number of training samples and to prevent too many network parameters, IAB leverages three layers of ResNet block and combines features with an average pooling layer. To make the numeralization of the infarct area intuitive, we integrate the area guidance knowledge of the infarct area, thus improving the sensitivity of DBSE-Net to the size of the infarct area.

IAB Summarized Advantages: Our newly proposed IAB effectively reduces the dimensionality of the lesion area features through simplified network structure and small receptive field. Through the high-weight infarct attention, the infarct area is enhanced without destroying the image structure. By the infarct area's guidance knowledge fusion mechanism, IAB accurately assesses the infarct area and solves the difficult identification of weak features to a certain extent.

4.4. The fully connection prediction layer

The fully connection prediction layer connects the impact of different single dimensions on the brain status (with or without infarct and compression), which enables global features and local features to impose different weights on HT's prediction (Fig. 3 - Sec4.4). Through HT lesions at two different scales, the layer fuses the local infarct area features and the global brain midline displacement features, thereby achieving higher-precision HT prediction.

5. Experimental Studies and Results

5.1. Data acquisition

We validated the performance of DBSE-Net by 144 intracranial stroke patients, diagnosed by doctors as low HT risk. All prediction results are derived from patients' clinical observations, and all segmentation labels are marked under the guidance of professional brain experts. Each frame image size is 512×512×1 with 40 window level, 80 window width. All patients had a cerebral infarction in the form of trial of org10172 in acute stroke treatment (TOAST)(Adams H P et al., 1993), but TPA was performed in all 144 intracranial stroke patients. The age distribution of TOAST patients was 70.06 as the mean and 11.30 as the standard deviation. All patients have

uneven distribution of infarct areas, and only a small number of patients have large infarct areas. We selected two frames of non-contrast images as a dual-channel image input obtained by the ASPECTS indicator.

5.2. Implementation details

We implement the construction and result testing of neural networks through the Python-based Pytorch library. The experimental environment is Linux (Ubuntu 18.04.1 LTS) desktop computer, equipped with TITAN X (PASCAL) graphics card and 390.48 Nvidia driver. The system memory is 16GB, and the CPU is Intel(R) Core(TM) i7-4790K. The optimizer selected in the experiment is ADAM (lr=0.001, weight_decay=5e-4). To improve experimental credibility, we apply a 5-fold cross-validation method during the experiment. In VW-UNet, we use the standard U-Net model, and the loss weight hyperparameter k of the infarct region is set to 3. In the IAB's infarct area attention mechanism, λ is set to 2 to enhance the local infarct area. To prevent over-fitting, we add a dropout mechanism to the ResNet block the last layer, with a coefficient of 0.7, and the dilated rate in BCAB is set to 2.

5.3. Prediction evaluation index

1) The precision, recall, and accuracy indicators are applied to evaluate the DBSE-Net prediction effect. 2) The kappa statistic is used to measure the agreement of the HT prediction result. 3) The receiver operating characteristic (ROC) curve with the area under ROC curve (AUC) and precision-recall (PR) curve are applied to compare with other scholars' methods. 4) The F_1 Score is proposed to balance precision and recall, which is defined as:

$$F_1 = 2 \cdot \frac{precision \cdot recall}{precision + recall} \tag{3}$$

where precision and recall are defined as:

$$precision = \frac{TP}{TP + FP} \tag{4}$$

$$recall = \frac{TP}{TP + FN} \tag{5}$$

where TP denotes true positive (network prediction is HT, the actual result is HT), FP denotes false positive (network prediction is HT, the actual result is normal), FN denotes false negative (network prediction is normal, the actual result is HT).

5.4. Segmentation evaluation index

1) We first use the most common evaluation indicator: dice coefficient to evaluate the brain region segmentation layer, which is the common indicator to compare with other models. Dice coefficient's result is in the range of [0-1]. The closer the result is to 1, the better the segmentation effect. Dice coefficient is defined as:

$$Dice = \frac{2 \cdot |X \cap Y|}{|X| + |Y|} \times 100\% \tag{6}$$

where X represents the region in the ground truth, Y represents the region in our network segmentation result.

2) Mean intersection over union (mIoU) metric is proposed to averagely evaluate the segmentation status of each category (infarction, left and right brain). The segmentation accuracy range of mIoU is 0-1, where 1 is the perfect segmentation situation(Tam et al., 2020). The mIoU formula is:

$$mIoU = \frac{1}{k+1} \sum_{i=0}^{k} \frac{|X_k \cap Y_k|}{|X_k \cup Y_k|} \tag{7}$$

where k represents the number of categories for segmentation tasks.

3) Kappa statistic is proposed to determine whether the label and the segmentation network output conform to the consistent distribution, the kappa statistic is defined as:

$$kappa = \frac{p_o - p_e}{1 - p_e} \tag{8}$$

where p_o represents the accuracy (number of pixels correctly classified), p_e is defined as:

$$p_e = \frac{P \cdot (TP + FN) + N \cdot (FP + TN)}{(P + N)^2} \tag{9}$$

where P represents the number of positive samples segmented by the network, N represents the number of negative samples segmented by the network. The range of the kappa score is [0,1], and a large kappa statistic indicates better agreement.

Table 1: Horizontal Comparison: The prediction evaluation table points out that DBSE-Net far exceeds traditional neural networks, and can assist doctors in the second HT risk diagnosis.

Method	Precision	Recall	Acc	F_1 Score	Kappa
DenseNet	0.5903	0.7500	0.5263	0.6587	-0.0877
ResNet	0.6623	0.6643	0.5833	0.6615	0.1176
SENet	0.5990	0.6286	0.5132	0.6130	-0.0428
DBSE-Net	**0.7348**	**0.8571**	**0.7193**	**0.7902**	**0.3737**

5.5. Comparison Experiments

Horizontal Comparison Experiment - DBSE-Net: Since no other scholars use non-contrast CT for HT prediction, a horizontal comparison is proposed to evaluate the performance difference between DBSE-Net and common classification networks: ResNet, DenseNet, SENet, which is the winner of the 2017 ILSVR competition. All classification networks use two ASPECTS images as input like DBSE-Net. Table 1 shows the horizontal comparison experiment results of DBSE-Net and common classification neural network models. The results show that traditional neural networks can hardly predict HT from non-contrast CT. Since traditional neural networks mainly classify images based on rich semantic information, but medical image has few semantic information. It is difficult for traditional neural networks to perform well with a relative lack of semantic information and high prediction difficulty. The accuracy rate of about 55% points out that traditional neural networks cannot extract useful brain lesion features, while DBSE-Net can extract sufficient brain structural abnormalities, thereby realizing HT's effective prediction. The 0-0.1 kappa statistics of the traditional neural network also shows that its prediction results are not consistent with the real results. The 0.3737 kappa statistics of DBSE-Net indicate that the predicted results meet the general consistency with the real patient situation. Fig. 5(a) and Fig. 5(b) respectively show the ROC and PR curve from the horizontal comparison experiment, which also proves that DBSE-Net can analyze non-contrast CT to predict HT.

Horizontal Comparison Experiment - ASPECTS Selection Rules: Although we explained the importance of the ASPECTS criterion for feature extraction, there is still a necessity for performance verification from a technical perspective. We perform two frames image offset on each input image selected by the ASPECTS criteria. Based on other experiment con-

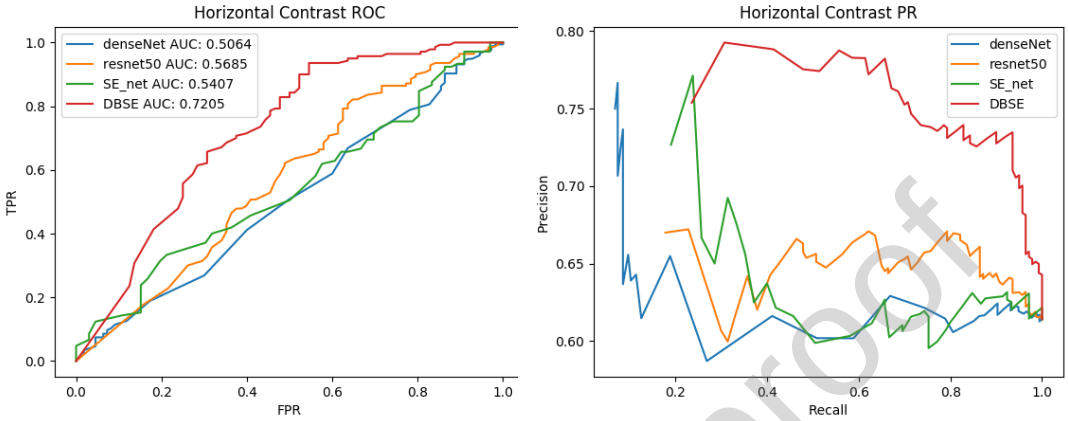

(a) Horizontal Comparison ROC (b) Horizontal Comparison PR

Figure 5: ROC and PR curves show that DBSE-Net has a good performance for HT prediction with non-contrast CT.

Table 2: Horizontal Comparison: The prediction results show that the precise selection of ASPECTS can increase about 5% prediction accuracy.

Method	Acc-Offset	Acc-NonOffset	Improvement
DenseNet	0.5213	0.5263	0.96%
ResNet	0.5428	0.5833	**7.46%**
SENet	0.5156	0.5132	-0.47%
DBSE-Net	**0.6837**	**0.7193**	5.21%

ditions unchanged, test the prediction performance of the baseline network and DBSE-Net.

The prediction results after image offset are shown in Table 2. The small infarct area may not be captured in non-key frames, and the brain structure may be unclear with slight image offset. Table 2 shows that the precise selection of ASPECTS can improve the prediction accuracy to a certain extent.

Horizontal Comparison Experiment - Brain region segmentation layer: We evaluate the brain region segmentation layer's separation effect on the left brain, right brain, and infarct region. Since the segmentation layer determines the accuracy of subsequent feature extraction and area guidance knowledge, the segmentation accuracy needs to be accurately assessed.

Quantitative results in terms of dice coefficient and mIoU are demonstrated in Table 3. As shown in the table, most networks have a good per-

Table 3: Horizontal Comparison: Multiple segmentation evaluations show that VW-UNet has the best segmentation effect and the highest consistency with label data.

	Dice	mIoU	Kappa
DeeplabV3(Chen et al., 2017)	0.9632	0.9609	0.9846
DeeplabV3+(Chen et al., 2018)	0.9554	0.9508	0.9770
PSPNet(Zhao et al., 2017)	0.9602	0.9575	0.9822
UNet(Ronneberger et al., 2015)	0.9657	0.9634	0.9857
VW-UNet	**0.9706**	**0.9644**	**0.9876**

formance on the brain segmentation, and VW-UNet is the most prominent network. Simultaneously, the ultra-high kappa statistic also points out that the segmentation network result is remarkably consistent with the original label.

The segmentation results from different networks are shown in Fig. 6. From sample 1 and sample 2, VW-UNet is the network with the highest fit to the infarct area among all networks. From sample 3, DeeplabV3 and UNet mis-segments brain tissue: sylvian fissure, not the infarct area while VW-UNet does not mis-segment. From sample 4, only VW-UNet successfully segmented the infarct area. From sample 5, for multi-region infarct region segmentation, UNet successfully segmented one of the infarct regions, but only VW-UNet successfully segmented all infarct regions. From all the samples, UNet and VW-UNet have the best segmentation effect on brain regions. However, VW-UNet has a better segmentation effect on the infarct area, but has a small part of brain tissue region mis-segmentations.

Ablation Comparison Experiment - Brain region segmentation layer: To test the effectiveness of VW-UNet in prediction task, we choose the traditional segmentation network to replace VW-UNet to implement ablation experiments (Table 4). In Table 4, VW-UNet has the best adaptability to DBSE-Net. Different networks' prediction effects have little difference in prediction tasks. Although UNet has the highest recall value and PSPNet has the highest precision value, VW-UNet has the best AUC and accuracy for the prediction task. VW-UNet increases the weight of the infarct area and improves the accuracy of the key information about the infarct area, which is more in line with infarct assessment. Fig. 7(a) and Fig. 7(b) respectively show the ROC and PR curve about the brain region segmentation layer ablation experiment. Through ROC and PR curves, the effectiveness of VW-UNet can be visually demonstrated.

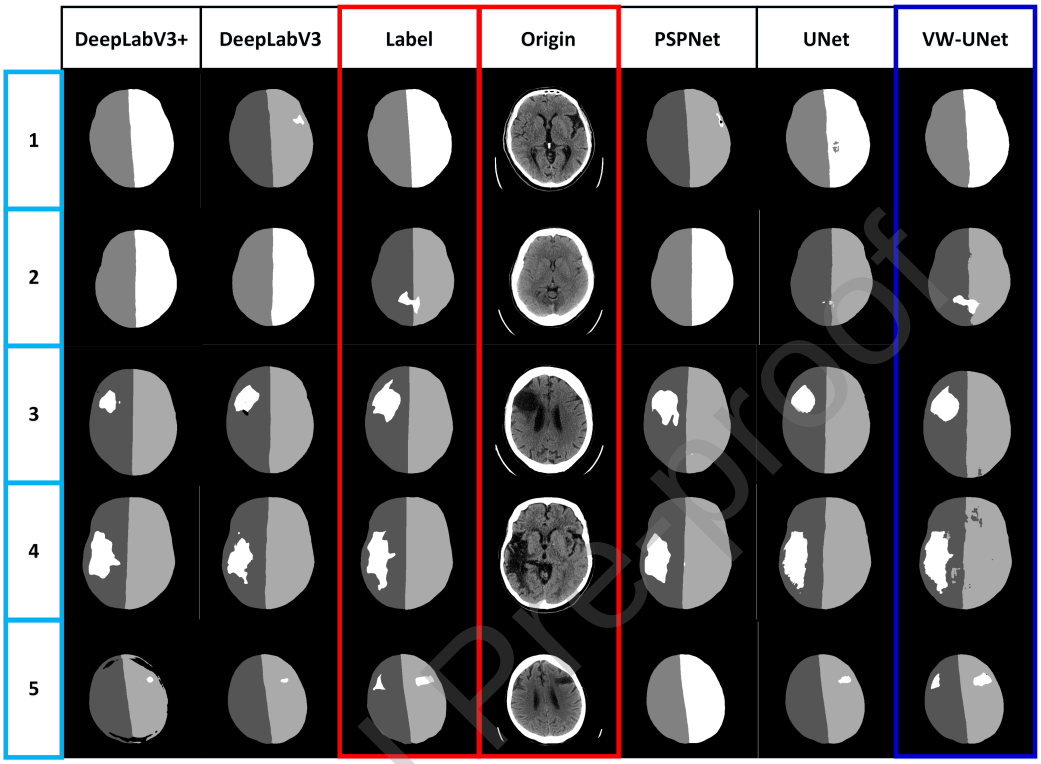

Figure 6: Comparison of segmentation effects of brain region segmentation layer: The segmentation output results show that VW-UNet focuses more on the infarct area and performs better under complex infarct shapes.

Table 4: Ablation Comparison: Replacing VW-UNet with traditional segmentation networks. The effectiveness of VW-UNet is verified by different networks' prediction results. Among all networks, the most suitable brain region segmentation layer for DBSE-Net is VW-UNet.

Seg Layer	Precision	Recall	Acc	F_1 Score	Kappa
PSPNet	**0.7593**	0.7929	0.7061	0.7634	0.3667
DeepLabV3	0.7209	0.8429	0.7018	0.7764	0.3362
DeepLabV3P	0.7201	0.8214	0.6930	0.7665	0.3230
UNet	0.7199	**0.8857**	0.7105	0.7892	0.3363
VW-UNet	0.7348	0.8571	**0.7193**	**0.7902**	**0.3737**

Ablation Comparison Experiment - Feature Encoding layer: We use the traditional prediction neural network to test the necessity of the dual-branch encoding layer. As shown in Table 5, the DBSE-Net encoding

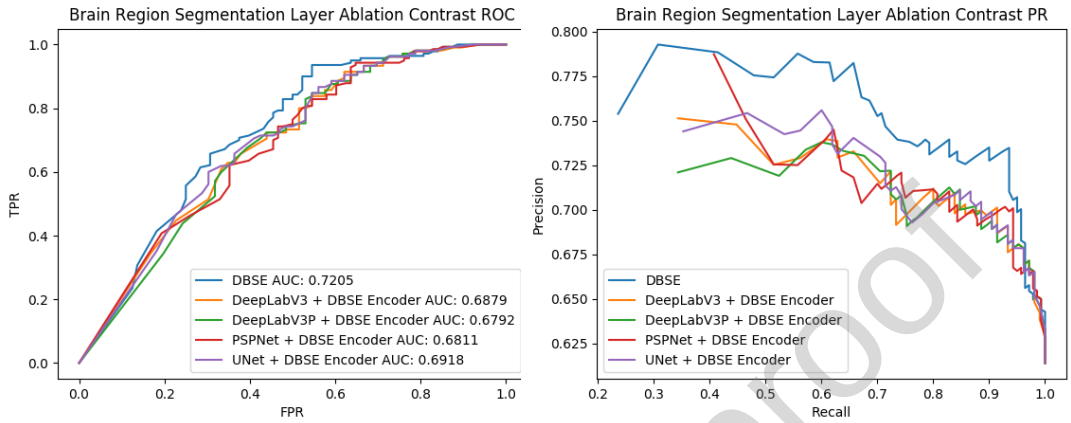

(a)Ablation Comparison ROC (b) Ablation Comparison PR

Figure 7: ROC and PR curves show that VW-UNet is the most suitable substructure for DBSE-Net.

Table 5: Ablation Comparison: Replace dual-branch feature encoding layer with traditional classification encoder networks. Verify the dual-branch feature encoding layer's effectiveness based on the prediction effect of the overall network. The results show that the IAB+BCAB encoding structure is most suitable for DBSE-Net.

Encoder	Precision	Recall	Acc	F_1 Score	Kappa
DenseNet	0.6337	0.8214	0.5877	0.7008	0.0343
SENet	0.6906	0.6571	0.5789	0.6340	0.1063
ResNet	0.7271	0.7714	0.6798	0.7475	0.3101
IAB+BCAB	**0.7348**	**0.8571**	**0.7193**	**0.7902**	**0.3737**

layer is compared with DenseNet, ResNet and SEnet. In this experiment, the input of the traditional neural network is a four-channel ASPECTS non-contrast CT image. The four channel image is the superposition of the brain region segmentation layer output and the DBSE-Net original input image. As shown in Table 5, DenseNet and SEnet are not suitable for the feature encoding task of HT prediction. Compared with Table 1, ResNet uses a pre-segmentation network to greatly improve the prediction effect. However, the joint feature encoding structure of IAB+BCAB exceeds the single encoding structure of ResNet in all aspects, and becomes the most suitable feature encoding structure for DBSE-Net. To clearly describe the differences between the various networks, we also used the ROC and PR curves in Fig. 8(a) and

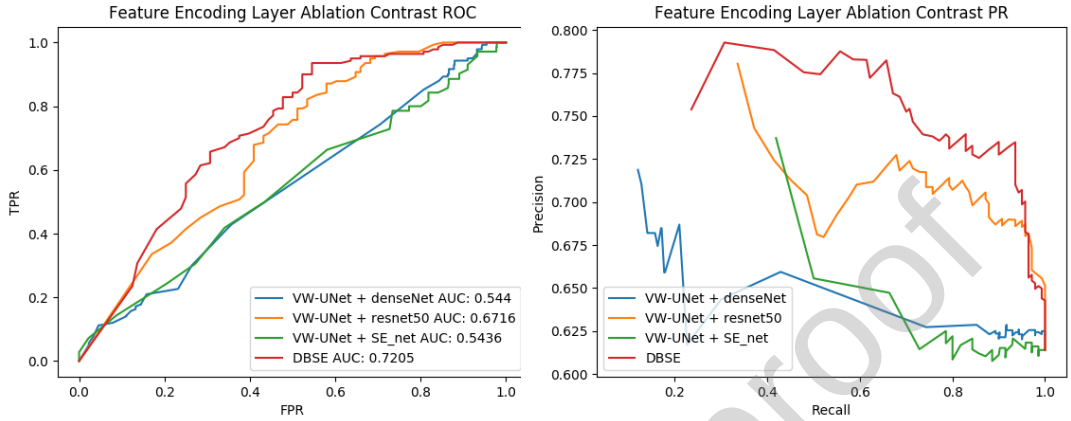

(a) Ablation Comparison ROC (b) Ablation Comparison PR

Figure 8: ROC and PR show that the IAB+BCAB encoder is most suitable for the DBSE-Net structure.

Table 6: Ablation Comparison: DBSE-Net is compared with the effect of retaining only a single branch. The experimental results show that the single branch is not suitable for HT prediction mode, and only the dual branch of IAB+BCAB can achieve accurate HT prediction.

DBSE		Precision	Recall	Acc	F_1	Kappa
BCAB	IAB					
✓		0.6947	0.7143	0.6316	0.7038	0.2162
	✓	0.6598	0.7286	0.6001	0.6914	0.1290
✓	✓	0.7348	0.8571	0.7193	0.7902	0.3737

Fig. 8(b).

Ablation Comparison Experiment - IAB & BCAB: To test the effectiveness of each branch, we apply an ablation experiment to detect local branch and global branch separately, which is shown in Tabel 6. The table shows that the BCAB global branch has a significant improvement in the prediction of HT. Due to the introduction of area guidance knowledge and the guidance of pre-segmented regions, the BCAB global branch focuses on distinguishing the infarct area and whether the brain area has a midline displacement phenomenon. On the contrary, the improvement of the IAB local branch is limited. Compared with traditional neural networks, the assistance of area guidance knowledge and network structure optimization make local

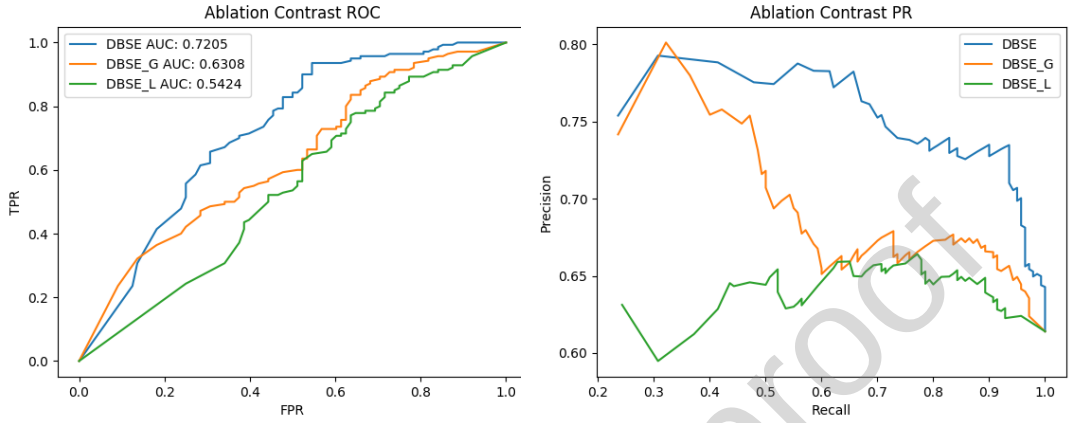

(a) Ablation Comparison ROC (b) Ablation Comparison PR

Figure 9: The ablation comparison curve between DBSE-Net and its respective branches. DBSE_G means to reserve the BCAB branch (Global), DBSE_L means to reserve the IAB branch (Local). ROC and PR results show that only the dual-branch combination of IAB+BCAB can achieve accurate HT prediction.

branches still have HT prediction ability. It can be seen from kappa statistics that BCAB and IAB branches have a poor correlation with HT's prediction results. However, the DBSE-Net combines the BCAB branch and the IAB branch, making the two branch networks complementary, thereby achieving HT prediction on non-contrast CT. From the perspective of DBSE-Net's high recall index, DBSE-Net is inclined to conservative HT treatment, which is also in line with the medical community's current status to avoid high HT risks. For a clear description of the DBSE-Net's each branch performance, the ROC curve and the PR curve are presented in Fig. 9(a) and Fig. 9(b).

To describe the effectiveness of the network structure and explain the intermediate feature information of the DBSE-Net, the intermediate feature map is presented in Fig. 10. The feature results of L_Layer1 and L_Layer2 can clearly show that the global branch focuses on the infarct location, the area of the infarct, and the boundary between the left and right brains. According to the segmentation results and the performance of L_Layer1, the local branch's pre-feature extraction entirely depends on the accuracy of the segmentation network. From the performance of G_Layer1 and G_Layer2, the local branch pays more attention to the infarct details and the brain tissue features (brain compression).

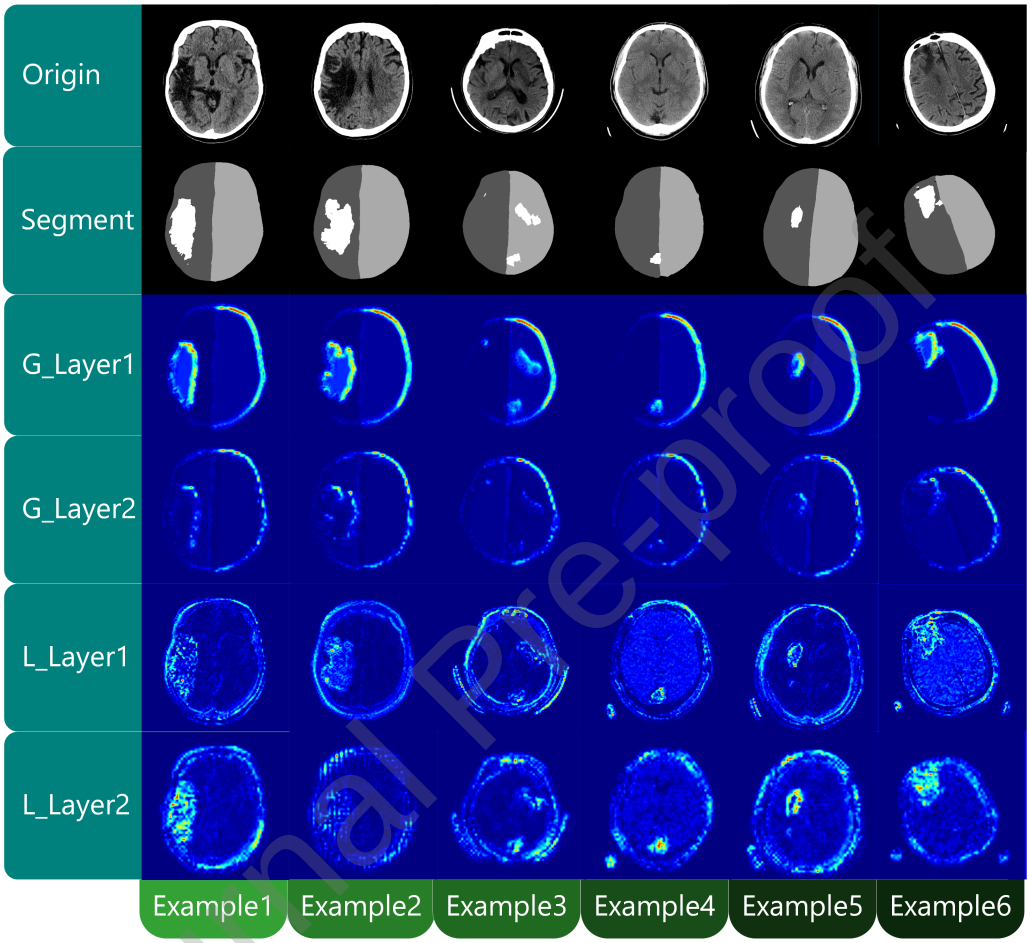

Figure 10: DBSE-Net's dual-branch middle layer output heat map. G_Layer means the BCAB branch layer, L_Layer means the IAB branch layer. The heat map shows that each layer of the DBSE-Net effectively pays attention to the infarct area and the global brain compression.

6. Discussion and conclusion

In this paper, our main contribution is that, for the first time, we achieve HT prediction based on non-contrast CT, which is difficult and of great medical significance. The non-contrast CT-based HT prediction method can effectively reduce the possibility of the patient being injured by the perfusion agent and save the economic cost, labor cost, and time cost. Our framework is built on a dual-branch feature separation and enhanced neural network

(DBSE-Net) to achieve the accurate HT prediction. The dual branch separation and enhancement mechanism in DBSE-Net effectively extract the multi-category and multi-scale lesion features. Simultaneously, DBSE-Net solves the poor relationship problem through adaptive feature encoding and introduction of guidance knowledge. Based on the redundant information removal of the ASPECTS keyframe selection layer, DBSE-Net enhances the keyframe lesion features. Relying on the adaptive feature encoding structure (BCAB and IAB) and VW-UNet which pays more attention to the infarct area, DBSE-Net effectively extracts weak lesion features. DBSE-Net solves the problems of poor relationship and weak feature extraction, thus realizing accurate HT prediction. The prediction accuracy (0.72 to 0.55±0.03) and kappa statistics (0.37 to 0.02±0.09) far exceeding that of the conventional classification network demonstrate the effectiveness of DBSE-Net.

In summary, we use 288 non-contrast CT images from 144 patients to achieve an accurate preliminary prediction of HT. Previous research works do not choose HT prediction based on non-contrast CT, which is realized by our study. Through our non-contrast CT prediction method, a large number of high-risk HT patients will be rescued. We hope that in the future, non-contrast CT prediction algorithms with higher accuracy and better prediction effect can be proposed to save patients' lives.

Declaration of interests

The authors declare that they have no known competing financial interests or personal relationships that could have appeared to influence the work reported in this paper.

References

Adams H P, Bendixen B H, Kappelle L J, Biller J, Love B B, Gordon D L, Marsh E E, 1993. Classification of subtype of acute ischemic stroke. Definitions for use in a multicenter clinical trial. TOAST. Trial of Org 10172 in Acute Stroke Treatment. Stroke 24, 35–41. URL: https://www.ahajournals.org/doi/abs/10.1161/01.str.24.1.35, doi:10.1161/01.STR.24.1.35. publisher: American Heart Association.

Aviv, R.I., d'Esterre, C.D., Murphy, B.D., Hopyan, J.J., Buck, B., Mallia, G., Li, V., Zhang, L., Symons, S.P., Lee, T.Y., 2009. Hemorrhagic Trans-

formation of Ischemic Stroke: Prediction with CT Perfusion. Radiology 250, 867–877. URL: https://pubs.rsna.org/doi/full/10.1148/radiol.2503080257, doi:10.1148/radiol.2503080257. publisher: Radiological Society of North America.

Bang, O.Y., Buck, B.H., Saver, J.L., Alger, J.R., Yoon, S.R., Starkman, S., Ovbiagele, B., Kim, D., Ali, L.K., Sanossian, N., Jahan, R., Duckwiler, G.R., Viñuela, F., Salamon, N., Villablanca, J.P., Liebeskind, D.S., 2007. Prediction of hemorrhagic transformation after recanalization therapy using T2*-permeability magnetic resonance imaging. Annals of Neurology 62, 170–176. URL: https://onlinelibrary.wiley.com/doi/abs/10.1002/ana.21174, doi:10.1002/ana.21174. _eprint: https://onlinelibrary.wiley.com/doi/pdf/10.1002/ana.21174.

Barbier, E.L., Lamalle, L., Décorps, M., 2001. Methodology of brain perfusion imaging. Journal of Magnetic Resonance Imaging: An Official Journal of the International Society for Magnetic Resonance in Medicine 13, 496–520.

Bouts, M.J., Tiebosch, I.A., Rudrapatna, U.S., van der Toorn, A., Wu, O., Dijkhuizen, R.M., 2017. Prediction of hemorrhagic transformation after experimental ischemic stroke using MRI-based algorithms. Journal of Cerebral Blood Flow & Metabolism 37, 3065–3076. URL: https://doi.org/10.1177/0271678X16683692, doi:10.1177/0271678X16683692. publisher: SAGE Publications Ltd STM.

Broocks, G., Flottmann, F., Scheibel, A., Aigner, A., Faizy, T.D., Hanning, U., Leischner, H., Broocks, S.I., Fiehler, J., Gellissen, S., et al., 2018. Quantitative lesion water uptake in acute stroke computed tomography is a predictor of malignant infarction. Stroke 49, 1906–1912.

C, O., Y, S., D, D., S, C., R, M., G, R., D, F., C, M., 2002. DWI prediction of symptomatic hemorrhagic transformation in acute MCA infarct. Journal of Neuroradiology = Journal de Neuroradiologie 29, 6–13. URL: https://europepmc.org/article/med/11984472.

Chen, L.C., Papandreou, G., Schroff, F., Adam, H., 2017. Rethinking atrous convolution for semantic image segmentation. arXiv preprint arXiv:1706.05587 .

Chen, L.C., Zhu, Y., Papandreou, G., Schroff, F., Adam, H., 2018. Encoder-decoder with atrous separable convolution for semantic image segmentation, in: Proceedings of the European conference on computer vision (ECCV), pp. 801–818.

Hu, J., Shen, L., Sun, G., 2018. Squeeze-and-excitation networks, in: Proceedings of the IEEE conference on computer vision and pattern recognition, pp. 7132–7141.

Huang, G., Liu, Z., Van Der Maaten, L., Weinberger, K.Q., 2017. Densely connected convolutional networks, in: Proceedings of the IEEE conference on computer vision and pattern recognition, pp. 4700–4708.

Hunter, G.J., Hamberg, L.M., Ponzo, J.A., Huang-Hellinger, F.R., Morris, P.P., Rabinov, J., Farkas, J., Lev, M.H., Schaefer, P.W., Ogilvy, C.S., et al., 1998. Assessment of cerebral perfusion and arterial anatomy in hyperacute stroke with three-dimensional functional ct: early clinical results. American Journal of Neuroradiology 19, 29–37.

Hutchinson, M.L., Beslow, L.A., 2019. Hemorrhagic Transformation of Arterial Ischemic and Venous Stroke in Children. Pediatric Neurology 95, 26–33. URL: http://www.sciencedirect.com/science/article/pii/S0887899418313006, doi:10.1016/j.pediatrneurol.2019.01.023.

Kim, E.Y., Na, D.G., Kim, S.S., Lee, K.H., Ryoo, J.W., Kim, H.K., 2005. Prediction of Hemorrhagic Transformation in Acute Ischemic Stroke: Role of Diffusion-Weighted Imaging and Early Parenchymal Enhancement. American Journal of Neuroradiology 26, 1050–1055. URL: http://www.ajnr.org/content/26/5/1050. publisher: American Journal of Neuroradiology Section: BRAIN.

Knight, R.A., Barker, P.B., Fagan, S.C., Li, Y., Jacobs, M.A., Welch, K.M.A., 1998. Prediction of impending hemorrhagic transformation in ischemic stroke using magnetic resonance imaging in rats. Stroke 29, 144–151. URL: https://jhu.pure.elsevier.com/en/publications/prediction-of-impending-hemorrhagic-transformation-in-ischemic-st-4, doi:10.1161/01.STR.29.1.144. publisher: Lippincott Williams and Wilkins.

Larrue, V., von Kummer, R., del Zoppo, G., Bluhmki, E., 1997. Hemorrhagic transformation in acute ischemic stroke: potential contributing factors in the european cooperative acute stroke study. Stroke 28, 957–960.

Lin, K., Kazmi, K.S., Law, M., Babb, J., Peccerelli, N., Pramanik, B.K., 2007. Measuring Elevated Microvascular Permeability and Predicting Hemorrhagic Transformation in Acute Ischemic Stroke Using First-Pass Dynamic Perfusion CT Imaging. American Journal of Neuroradiology 28, 1292–1298. URL: http://www.ajnr.org/content/28/7/1292, doi:10.3174/ajnr.A0539. publisher: American Journal of Neuroradiology Section: BRAIN.

Mozaffarian, D., Benjamin, E.J., Go, A.S., Arnett, D.K., Blaha, M.J., Cushman, M., De Ferranti, S., Després, J.P., Fullerton, H.J., Howard, V.J., et al., 2015. Executive summary: heart disease and stroke statistics—2015 update: a report from the american heart association. Circulation 131, 434–441.

Neumann-Haefelin C., Brinker G., Uhlenküken U., Pillekamp F., Hossmann K-A., Hoehn M., 2002. Prediction of Hemorrhagic Transformation After Thrombolytic Therapy of Clot Embolism. Stroke 33, 1392–1398. URL: https://www.ahajournals.org/doi/full/10.1161/01.str.0000014619.59851.65, doi:10.1161/01.STR.0000014619.59851.65. publisher: American Heart Association.

of Neurological Disorders, N.I., rt PA Stroke Study Group, S., 1995. Tissue plasminogen activator for acute ischemic stroke. New England Journal of Medicine 333, 1581–1588.

Pexman, J.W., Barber, P.A., Hill, M.D., Sevick, R.J., Demchuk, A.M., Hudon, M.E., Hu, W.Y., Buchan, A.M., 2001. Use of the alberta stroke program early ct score (aspects) for assessing ct scans in patients with acute stroke. American Journal of Neuroradiology 22, 1534–1542.

Qiu, W., Kuang, H., Teleg, E., Ospel, J.M., Sohn, S.I., Almekhlafi, M., Goyal, M., Hill, M.D., Demchuk, A.M., Menon, B.K., 2020. Machine learning for detecting early infarction in acute stroke with non–contrast-enhanced ct. Radiology 294, 638–644.

Ronneberger, O., Fischer, P., Brox, T., 2015. U-net: Convolutional networks for biomedical image segmentation, in: International Conference on Medical image computing and computer-assisted intervention, Springer. pp. 234–241.

Sussman, E.S., Connolly Jr, E.S., 2013. Hemorrhagic transformation: a review of the rate of hemorrhage in the major clinical trials of acute ischemic stroke. Frontiers in neurology 4, 69.

Szegedy, C., Ioffe, S., Vanhoucke, V., Alemi, A., 2016. Inception-v4, inception-resnet and the impact of residual connections on learning. arXiv preprint arXiv:1602.07261 .

Tam, C.M., Zhang, D., Chen, B., Peters, T., Li, S., 2020. Holistic multitask regression network for multiapplication shape regression segmentation. Medical Image Analysis 65, 101783.

Wang, Q., Reps, J.M., Kostka, K.F., Ryan, P.B., Zou, Y., Voss, E.A., Rijnbeek, P.R., Chen, R., Rao, G.A., Stewart, H.M., Williams, A.E., Williams, R.D., Zandt, M.V., Falconer, T., Fernandez-Chas, M., Vashisht, R., Pfohl, S.R., Shah, N.H., Kasthurirathne, S.N., You, S.C., Jiang, Q., Reich, C., Zhou, Y., 2020. Development and validation of a prognostic model predicting symptomatic hemorrhagic transformation in acute ischemic stroke at scale in the OHDSI network. PLOS ONE 15, e0226718. URL: https://journals.plos.org/plosone/article?id=10.1371/journal.pone.0226718, doi:10.1371/journal.pone.0226718. publisher: Public Library of Science.

Wiley, G., 2008. The new economics of contrast. https://www.radiologybusiness.com/topics/business-intelligence/new-economics-contrast. Accessed September 02, 2008.

Xu, C., Zhang, D., Chong, J., Chen, B., Li, S., 2021. Synthesis of gadolinium-enhanced liver tumors on nonenhanced liver mr images using pixel-level graph reinforcement learning. Medical Image Analysis 69, 101976.

Yassi Nawaf, Parsons Mark W., Christensen Søren, Sharma Gagan, Bivard Andrew, Donnan Geoffrey A., Levi Christopher R., Desmond Patricia M., Davis Stephen M., Campbell Bruce C.V., 2013. Prediction of Poststroke

Hemorrhagic Transformation Using Computed Tomography Perfusion. Stroke 44, 3039–3043. URL: https://www.ahajournals.org/doi/full/10.1161/strokeaha.113.002396, doi:10.1161/STROKEAHA.113.002396. publisher: American Heart Association.

Yen, P., Cobb, A., Shankar, J.J.S., 2016. Does computed tomography permeability predict hemorrhagic transformation after ischemic stroke? World Journal of Radiology 8, 594–599. URL: https://www.ncbi.nlm.nih.gov/pmc/articles/PMC4919759/, doi:10.4329/wjr.v8.i6.594.

Yu, Y., Guo, D., Lou, M., Liebeskind, D., Scalzo, F., 2018. Prediction of Hemorrhagic Transformation Severity in Acute Stroke From Source Perfusion MRI. IEEE Transactions on Biomedical Engineering 65, 2058–2065. doi:10.1109/TBME.2017.2783241. conference Name: IEEE Transactions on Biomedical Engineering.

Yu, Y., Parsi, B., Speier, W., Arnold, C., Lou, M., Scalzo, F., 2019. Lstm network for prediction of hemorrhagic transformation in acute stroke, in: International Conference on Medical Image Computing and Computer-Assisted Intervention, Springer. pp. 177–185.

Zhao, H., Shi, J., Qi, X., Wang, X., Jia, J., 2017. Pyramid scene parsing network, in: Proceedings of the IEEE conference on computer vision and pattern recognition, pp. 2881–2890.

Zhao, W., Zhang, J., Chen, J., Song, H., Ji, X., 2019. Net water uptake: a new tool for the assessment of ischaemic stroke oedema. Brain 142, e34–e34.

Declaration of interests

☒ The authors declare that they have no known competing financial interests or personal relationships that could have appeared to influence the work reported in this paper.

☐The authors declare the following financial interests/personal relationships which may be considered as potential competing interests:

CRediT authorship contribution statement

Ziqiao Wang: Conceptualization, Methodology, Software, Writing - Original Draft, Writing - Review and Editing.

Zhi Liu: Supervision, Project administration, Writing- Reviewing and Editing.

Shuo Li: Supervision, Project administration, Software, Writing- Reviewing and Editing, Data Curation, Investigation.

Highlights

Weak Lesion Feature Extraction by Dual-branch Separation and Enhancement Network for Safe Hemorrhagic Transformation Prediction

Ziqiao Wang, Zhi Liu, Shuo Li

- For the first time, we achieved a non-contrast CT-based HT prediction method, which is safe, free of secondary brain injury, low cost, and less workload
- A dual-branch feature separation and enhancement network (DBSE-Net) is proposed to model the relationship between lesions and HT prediction results
- Our proposed algorithm structure effectively solves the weak lesion feature problem

Weak Lesion Feature Extraction by Dual-branch Separation and Enhancement Network for Safe Hemorrhagic Transformation Prediction

Ziqiao Wang[a], Zhi Liu[a,*], Shuo Li[b]

[a]*School of Information Science and Engineering, Shandong University, Qingdao, 266237, China*

[b]*Digital Imaging Group of London, Western University, London, ON N6A 3K7, Canada*

Abstract

Hemorrhagic transformation (HT) is regarded as a safety endpoint of arterial ischemic stroke acute treatment and secondary prevention trials(Hutchinson and Beslow, 2019). Accurate HT prediction dramatically reduces the death rate from misdiagnosis. At present, HT predictions almost all rely on contrast images with perfusion agents, which is time-consuming and labor-intensive, causing secondary brain damage and high cost. Almost all machine learning algorithms cannot use non-contrast CT for HT prediction because of huge challenges. In this study, a Dual-branch Separation and Enhancement Network (DBSE-Net) is proposed for weak feature extraction and safe HT prediction without perfusion agents. DBSE-Net innovatively uses a dual-branch separation and fusion mechanism to achieve weak feature adaptive extraction. In the DBSE-Net's encoder submodules, Brain Compression Assessment Branch (BCAB) and Infarct Assessment Branch (IAB) are proposed to apply lightweight encoding structures with different receptive fields, which are adapted to the lesion area's characteristics. With the help of DBSE-Net's keyframe selection algorithm and area guidance knowledge, DBSE-Net removes redundant information and clearly describes the severity of lesions. In summary, DBSE-Net integrates global and local features to obtain multi-scale and multi-category brain status information, enhancing the weak features of non-contrast CT and realizes accurate HT prediction. Experimental Result:

*Corresponding author

Email address: liuzhi@sdu.edu.cn (Zhi Liu)

Among all 144 intracranial stroke patients diagnosed by doctors as having no HT risk, DBSE-Net identified 73 high-risk HT patients (88 HT cases in total). The result illustrates that DBSE-Net helps doctors secondary diagnose the HT risk of intracranial stroke patients and becomes a potential tool to prevent doctors from false HT risk diagnosis.

Keywords: Hemorrhagic transformation prediction, Non-contrast CT, DBSE-Net.

1. Introduction

The accurate prediction of hemorrhagic transformation (HT) can reduce the misdiagnosis rate of doctors and improve the survival rate of patients(Sussman and Connolly Jr, 2013). Nowadays, Hemorrhagic transformation (HT) is regarded as a safety endpoint of arterial ischemic stroke acute treatment and secondary prevention trials(Hutchinson and Beslow, 2019). As a common spontaneous complication after intracranial embolism, HT is easily misdiagnosed by doctors and leads to death. From 2001 to 2011, an average of 795,000 people produced a stroke or recurrent stroke (hemorrhagic or ischemic) annually in the United States, of which 185,000 people were recurrent stroke episodes(Mozaffarian et al., 2015). Doctors usually use tissue plasminogen activator (TPA) as a treatment for patients with infarction. However, if the doctor uses TPA treatment for stroke patients with high HT risk, the wrong treatment will lead to an increased HT phenomenon and even death(Larrue et al., 1997)(of Neurological Disorders and rt PA Stroke Study Group, 1995). The HT prediction method can perform an HT risk second diagnosis on stroke patients and correct the doctor's judgment. With the computer-aided HT prediction method, stroke patients with high HT risk will not use TPA treatment, which will cause secondary intracranial hemorrhage. As shown in Fig.1 (Clinical Significance), computer-aided HT prediction methods can help doctors confirm the patient's brain status and determine whether to use TPA treatment, which increases the patient's cure rate. Although there are many methods for evaluating the indicators of HT prediction, such as net water uptake (NWU)(Broocks et al., 2018)(Zhao et al., 2019), they only stop at the indicator evaluation without further systematic prediction of HT. At present, in the field of cerebrovascular accidents, there is an urgent need for an accurate, convenient, and low brain injury HT prediction method.

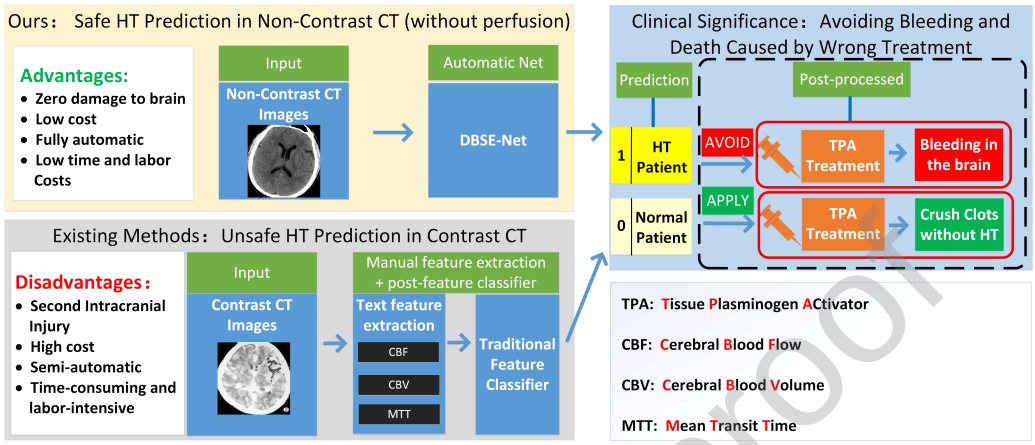

Figure 1: Significance of Predicting Hemorrhagic Transformation on Safe CT (Non-contrast)

The current HT prediction methods are based on contrast CT or contrast MRI, which have four major disadvantages (shown in Fig.1). **1)**Second Intracranial Injury: contrast CT/MRI image generation requires the injection of perfusion agents. The injected non-diffusion perfusion agents will change the relaxation time of the vascular bed in the adjacent tissue(Barbier et al., 2001), which destroys the already fragile blood vessel wall. The injection of perfusion agents eventually increases the likelihood of HT and causes other risks to patients with compromised kidney function(Xu et al., 2021). **2)**High Cost: the use of perfusion agents in CT/MRI images brings additional economic costs to patients. Contrast CT/MRI costs 1.5 times more than ordinary CT/MRI images(Wiley, 2008), making poor patients bear high economic pressure. **3)**Semi-automatic: Most existing HT prediction techniques require manual extraction of Cerebral Blood Flow (CBF), Cerebral Blood Volume (CBV), and Mean Transit Time (MTT)(Yu et al., 2019) vascular assessment features. These parameters are helpful for HT prediction but make the prediction network unable to realize fully automatic operation. **4)**Increase Time and Workload: Contrast CT also requires an additional CT scan, parameter calculation, and perfusion agent injection, which results in extra time on pathological examination. Existing Contrast CT requires continuous dynamic scanning of the region of interest (ROI) to find the perfusion agent response(Hunter et al., 1998).

Although Non-contrast CT has numerous advantages, Non-contrast CT

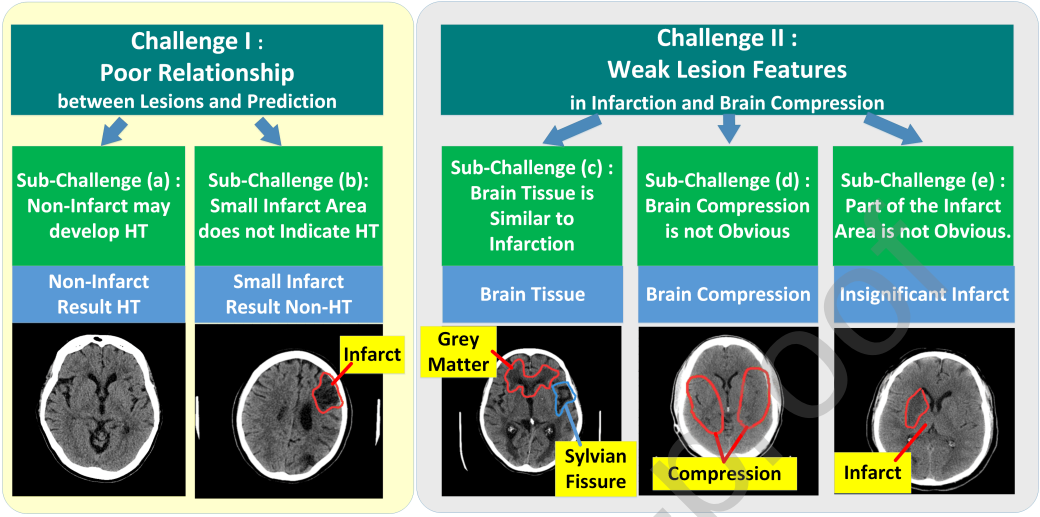

Figure 2: Challenges of safe non-contrast CT images without perfusion agent

is difficult to apply to HT prediction (Fig.2). For the non-contrast CT used for the HT prediction task, the two main challenges are as follows: **Firstly**, a poor relationship between lesion and prediction: There is no one-to-one relationship between the presence of cerebral infarction and HT in patients. In general, the larger the infarct size, the higher the possibility of HT. Nevertheless, some patients with HT do not have significant brain lesions in early diagnostic images. At the same time, patients with small infarcts in the brain do not develop HT. Like Fig. 2 (a), some patients have no obvious infarct area but develop HT results. In the Fig. 2 (b), small infarct area may not trigger HT phenomenon. **Secondary**, weak lesion features (insignificant lesions) in infarction and brain compression: Many lesions are difficult to distinguish visually, and the lesions are easily confused with brain tissue. As shown in Fig. 2 (c), the brain's inherent structure, grey matter, and sylvian are very similar to the infarct area. Not only external interference but also some lesion areas are difficult to observe, as shown in Fig. 2 (d). Brain compression manifests as an insignificant brain sulcus, but there is no clear evaluation index for insignificant sulcus. Furthermore, due to large differences in human brain structures, the infarct area is not significant for many patients. In Fig. 2 (e), the infarct area has little grey value different than the same position on the right brain region. Two major challenges indicate that HT prediction requires analysis of the brain's overall compression status and

the enhancement of local lesion features. The existing traditional neural network classification methods (ResNet(Szegedy et al., 2016), DenseNet(Huang et al., 2017), SE-Net(Hu et al., 2018)) are mainly based on the huge feature differences between semantic features. Simultaneously, traditional networks need a close relationship between image and prediction results. However, traditional networks are weak for medical image prediction tasks where semantic information is insufficient. Non-contrast CT images cannot clearly express future results is another problem for traditional neural networks.

This paper proposes a Dual-branch Separation and Enhancement Network (DBSE-Net) for HT prediction from non-contrast CT. DBSE-Net can correctly assess the deterioration of brain infarct area and brain compression, thereby achieving accurate prediction of HT. DBSE-Net is based on the principle that HT is associated with the intracranial infarct area and the brain's midline displacement status (intracranial compression status). Based on the principle, the overall framework of DBSE-Net proposes a dual-branch lesion region separation processing mechanism. DBSE-Net consists of four layers: 1) Concerning enormous useless frames of clinical CT images, the brain keyframe selection layer is proposed to extract two keyframe images from 64 non-contrast CT images based on Alberta stroke program early CT score (ASPECTS). 2) In the brain region segmentation layer, Variable Weight UNet (VW-UNet) is proposed to pre-segment brain regions and separate global and local features. VW-UNet uses an infarct-focused segmentation model to effectively pre-segment the brain region and obtain lesion guidance knowledge, solving the weak semantic feature information problem. 3) Simultaneously, the Brain Compression Assessment Branch (BCAB) and Infarct Assessment Branch (IAB) in the dual-branch feature encoding layer are introduced to encode features, accurately extracting and enhancing different forms of features. To accurately express the severity of lesions, the brain region segmentation layer extracts lesion guidance knowledge to guide BCAB's and IAB's encoding structure training. 4) Based on lesion region separation processing mechanism and fully connection prediction layer, multi-scale and multi-category weak features are extracted to achieve accurate HT prediction.

The contributions and advantages are shown as follows:

- For the first time, we achieved a non-contrast CT-based HT prediction method, which is safe, free of secondary brain injury, low cost, and less workload. The method saves the lives of intracranial stroke patients

who are misdiagnosed by doctors.

- A dual-branch feature separation and enhancement network (DBSE-Net) is proposed to model the relationship between lesions and HT prediction results. DBSE-Net enhances the relationship between images and prediction results through guiding knowledge and a dual-branch adaptive encoding mechanism (extracting multi-category and multi-scale features), and enable non-contrast CT for HT prediction.

- Our proposed algorithm structure effectively solves the weak lesion feature problem. In the interference removal aspect, DBSE-Net proposes the ASPECTS keyframe selection layer to obtain keyframe information of the lesion area, which effectively solves network overfitting. In the feature processing aspect, we propose a separating brain lesion features (VW-UNet) and adaptive encoding (BCAB and IAB) mechanism based on clinical criteria. By encoding different lesion ROI according to their characteristics, effective weak feature extracting is achieved.

2. Related Works

Our proposed DBSE-Net is the first neural network that uses non-contrast CT for HT prediction. Other scholars all use perfusion contrast CT/MRI to apply accurate HT prediction methods.

Clinical medicine field: (Knight et al., 1998) used male Wistar rats based on T1-weighted and T2-weighted MRI to prove that Gd-DTPA is a reliable predictor of HT. (Aviv et al., 2009) proved that the product map measurement of permeability surface area appears promising for HT prediction with AUC of 0.918, the sensitivity of 77%, and specificity of 94%. (Lin et al., 2007) also proved that elevated permeability by using first-pass PCT could predict subsequent HT. (Bang et al., 2007) explained the permeability images derived from pretreatment perfusion MRI source data might identify patients at risk for HT with a sensitivity result of 83% while (Yen et al., 2016) got 78.6%. (Neumann-Haefelin C. et al., 2002) pointed out that the key to HT prediction is the disturbance of the blood-brain barrier but not of other MR parameters. (Kim et al., 2005) investigation in 55 cases showed that early parenchymal enhancement is highly specific for HT. They also pointed out that early reperfusion and damage to the blood-brain barrier in ischemic tissue may also be associated with HT's appearance. Moreover, diffusion-weighted imaging lesion volumes and apparent diffusion coefficient

indexes had no strong relationship with HT. However, (C et al., 2002) also proposed: a measurement of minimum apparent diffusion coefficient (ADC) values within an acute middle cerebral artery (MCA) stroke can achieve high-risk predictions for HT. Relative cerebral blood flow, relative cerebral blood volume, and time to maximum multi-parameter prediction methods are also proposed by (Yassi Nawaf et al., 2013). Both (Broocks et al., 2018) and (Zhao et al., 2019) proposed that net water uptake (NWU) is an important indicator of the severity of lesions in the infarct area, and it is also helpful for subsequent HT prediction.

Machine learning field: In recent years, modeling analysis and machine learning are performed on HT predictions. Compared with traditional machine learning, (Yu et al., 2018)'s kernel spectral regression method has achieved the highest accuracy of 83.7±2.6%. (Wang et al., 2020) used the Lasso logistic regression prediction model to accurately predict HT on a vast dataset (621,178 patients) and obtained an AUC of 0.78. Meanwhile, (Bouts et al., 2017) adopted a generalized linear model and random forest predictive algorithms to achieve HT prediction based on MRI datasets, which achieved AUC results of 0.85±0.14 and 0.89±0.09 in the two experimental groups. (Yu et al., 2019) adopted the LSTM network based on PWI combined with DWI imaging features into a fully connected neural network and verified that its AUC-ROC of 89.4% on 155 acute stroke patients. In addition to the HT prediction method, (Qiu et al., 2020) uses the U-Net(Ronneberger et al., 2015) transfer learning in the infarct region segmentation based on non-contrast CT and integrates multiple image features into the random forest to achieve accurate segmentation of the infarct region. Although the current HT prediction accuracy rate based on contrast images has reached a satisfactory status, no one ever tried non-contrast for HT prediction.

3. Method overview

As shown in Fig.3, Dual-branch Separation and Enhancement Network (DBSE-Net) consists of four modules as shown below. The four innovative modules achieve accurate prediction of HT based on non-contrast CT by removing redundant information, the separation and fusion of features based on clinical conditions, the adaptive feature encoding structure, and the introduction of guidance knowledge.

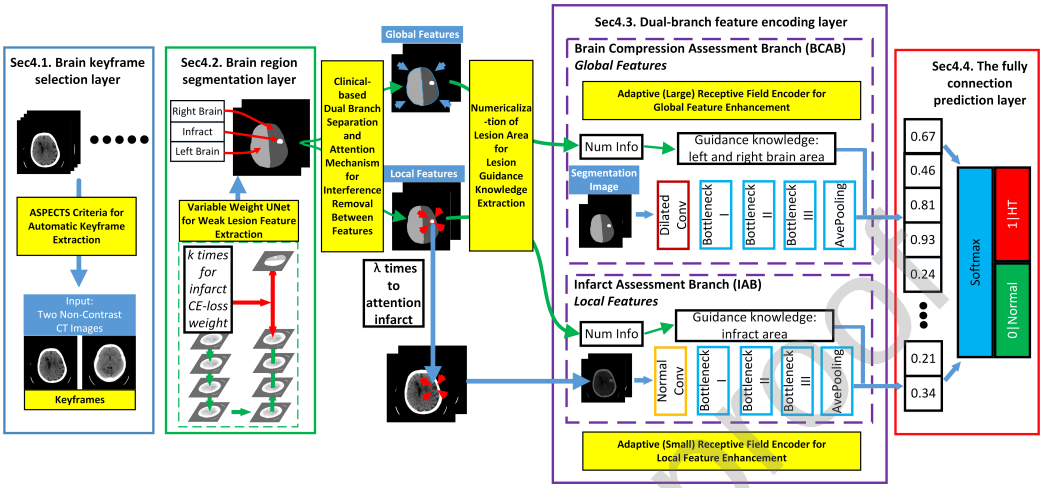

Figure 3: DBSE-Net Structure: Global and local brain feature separation for weak feature separation enhancement including: Sec4.1. brain keyframe selection layer, Sec4.2. brain region segmentation layer, Sec4.3. dual-branch feature encoding layer which consists of brain compression assessment branch (BCAB) and infarct assessment branch (IAB), Sec4.4. the fully connection prediction layer.

- **Brain keyframe selection layer enables automatic keyframe refinement.** The layer innovatively uses the Alberta stroke program early CT score (ASPECTS) medical evaluation index to extract two frames from sequence CT images. The layer selects keyframes in redundant information, reducing mutual interference between non-contrast CT images. Details are shown in sec4.1.

- **Brain region segmentation layer enables lesion area adaptive separation and guidance knowledge extraction.** The layer presegments the left brain, right brain, and infarct region to achieve the separation of the global and local image features. Simultaneously, the layer is based on variable weight training, which enhances the weak lesion features (infarct area). In the layer, the numerical guidance information extracted from the coverage lesion area assists the subsequent encoding network. By the separation of local and global features, the deterioration of the infarct area, the midline displacement, and the brain compression are revealed. Details are shown in sec4.2.

- **Dual-branch feature encoding layer enables adaptive enhancement and encoding of lesion features.** To effectively obtain the

low-dimensional information property of different scales, the module innovative performs guidance knowledge fusion, enhancement, and adaptive feature encoding of global features and local features. Details are shown in sec4.3.

- **The fully connection prediction layer for multi-feature fusion.** The module achieves HT's high-risk prediction by integrating the one-dimensional feature representations of local features, global features, guidance knowledge. Details are shown in sec4.4.

4. Methodology

4.1. Brain keyframe selection layer by ASPECTS medical evaluation index

Different from the direct input of the common 64-frame CT sequence, the brain keyframe selection layer innovatively uses the ASPECTS medical criterion as the keyframe image extraction method (Fig. 3 - Sec4.1), which keeps the brain structure status' main information content. The original 64-frame non-contrast CT images contain enormous irrelevant information without the lesion area. A large amount of irrelevant information causes the neural network to learn irrelevant information and cause serious overfitting. The layer innovatively uses the ASPECTS medical evaluation index to automatically extract two keyframes that can express all brain status. As shown in Fig. 4, the automatic extraction rules for ASPECTS images are: One at the level of the thalamus and basal ganglion (red arrow) and another adjacent to the most superior margin of the ganglionic structures (green arrow). Since the relative position of the two frames of images in the 64-frame CT sequence is roughly fixed, the two ASPECTS images can be automatically obtained from the CT sequence, which is collected from the same machine. Almost all the ASPECTS images are in fixed slices, but due to the different structure of the human brain, few images should be double checked in case there is an outlier. Neuroradiologists generally agree that the patient skull's pathological brain status can be obtained from two ASPECTS images(Pexman et al., 2001), proving the selection method is effective and in line with clinical criteria. With two keyframes, the brain lesion information of all 64-frame CT non-contrast images can be roughly obtained, avoiding the interference of enormous low-information images.

Summarized Advantages: The brain keyframe selection layer is based on ASPECTS criterion to extract two keyframes from 64 complex

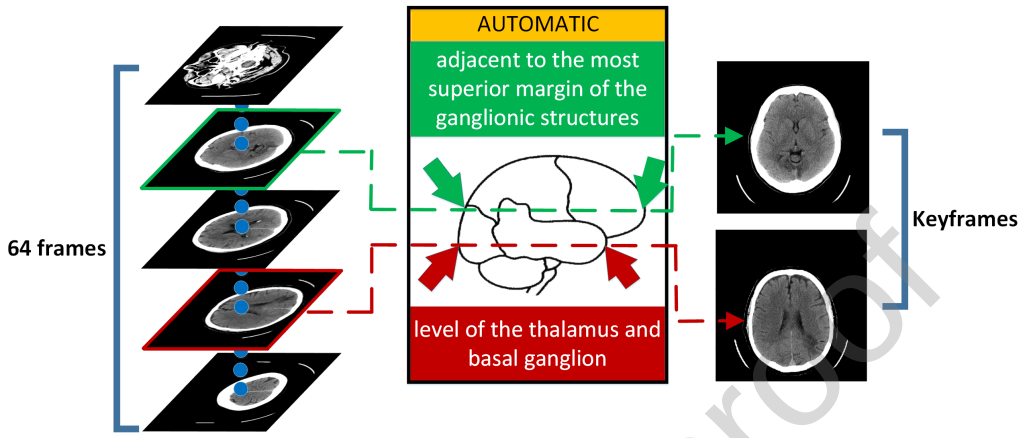

Figure 4: Schematic diagram of automatic brain keyframe selection method: CT frame extraction rules based on the Alberta stroke program early CT score.

non-contrast CT sequence images, which effectively removes redundant information according to clinicopathological characteristics.

4.2. Brain region segmentation layer by Variable Weight UNet

The brain region segmentation layer proposes Variable Weight UNet (VW-UNet) based on U-Net(Ronneberger et al., 2015) as a pre-segmentation network, which is suitable for small objects and multi-scale segmentation. The layer pre-segmentation of the three brain parts and acquisition of area guidance knowledge for the subsequent network structure (Fig. 3 - Sec4.2). From the many challenges of HT, the size of the infarct area is the core of HT prediction. Meanwhile, The characteristics of the infarct area are not significant and the midline displacement will occur between the left and right brains. Therefore, separate the infarct area from the left and right brains can accurately extract local detailed features. In VW-UNet, we input the two slices of ASPECTS images and manually label the left brain, right brain, and infarct area with a parenchymal hypoattenuation as VW-UNet training labels. Then we choose cross entropy as a loss function to train the classification results of each pixel point. Especially, to solve the infarct's weak and insignificant features, we increase the small objects (infarct) loss weight of VW-UNet by hyperparameter k times to make VW-UNet concerned about the effect of small object segmentation. In the follow-up layers, VW-UNet feeds BCAB the original segmentation image. Nevertheless, in the IAB, VW-UNet's local features weight the ASPECTS ori-images with hyperparameter λ to highlight

the infarct area importance as an attention mechanism. The formula of the attention is as follows:

$$I(i,j) = I(i,j) + \lambda * I(i,j) * S(i,j) \tag{1}$$

where I represents the IAB's input, λ represents the hyperparameter of attention mechanism. S is the brain keyframe selection layer's infarct class output (infarct segmentation image), and i, j are the pixel coordinates. Through the attention mechanism, the infarct area is highlighted so that the IAB brain local feature encoding structure focuses on the assessment of the infarct area.

Summarized Advantages: The brain region segmentation layer presegments the three brain regions through VW-UNet with a variable weight loss function, which improves the accurate segmentation of infarct regions with weak features. The layer separates the mixed global brain squeeze from the local infarct area for adaptive feature encoding. Simultaneously, the layer extracts guidance knowledge from the segmented image, solving the weak lesion features problem to a certain extent.

4.3. Dual-branch feature encoding layer by feature adaptive encoding network with different receptive fields

The dual-branch feature encoding layer obtains multi-scale and multi-category information (Fig. 3 - Sec4.3), which enriches the types of features, thereby solving the problem of weak features to a certain extent. The layer is divided into **Brain Compression Assessment Branch (BCAB)** and **Infarct Assessment Branch (IAB)**. Each branch integrates the area guidance knowledge and image features. The dual-branch separation, enhancement, and adaptive feature encoding strategy make features not interfere with each other and independently evaluate the brain status.

In BCAB, the image input is the segmentation result of the brain region segmentation layer, so as to realize the enhanced encoding of the weak brain compression feature. The receptive field of BCAB is increased to integrate the correlation between the overall structure. In the feature encoding structure, dilated convolution increases the receptive field without reducing the picture size so that BCAB subsequent structures can obtain long-ranged

information. The dilated convolution is defined as:

$$H(i,j) = \sum_{m=0}^{s-1}\sum_{n=0}^{s-1} K(m,n)G(i + \frac{(2m-s+1)\times dr}{2}, i + \frac{(2n-s+1)\times dr}{2}) \tag{2}$$

where H represents the convolution module's output, K represents the kernel of the convolution. s is expressed as the convolution kernel's size, while dr is expressed as the dilated rate. Through dilated convolution, BCAB focuses on the global structural features and brain compression state instead of local details, making BCAB assess the overall state of the brain.

In BCAB's subsequent feature encoding structure, ResNet blocks are selected to extract and generate feature maps. Average pooling is cascaded to integrate all overall brain structural features. Simultaneously, to prevent over-fitting caused by a deep layer network and numerous parameters, the ResNet block retains three layers. The area guidance knowledge is merged into the last layer of BCAB in the form of text, highlighting the midline displacement caused by the left and right brains' unequal brain area. By highlighting the brain structure, the BCAB focuses on the overall brain area's structural characteristics, selected to diagnose whether there are dangerous symptoms such as brain area deformation and blood vessel compression.

BCAB Summarized Advantages: Our newly proposed BCAB innovative provides a large-receiving field and lightweight feature encoding for global feature adaptive encoding. Through the single-dimensional feature fusion of guidance knowledge, BCAB integrates brain compression features, enhances the relationship of the weak features, and solves the phenomenon of weak features to a certain extent.

In IAB, the original ASPECTS image after attention is used as input to achieve enhanced encoding of the infarct area. A small receptive field encoder and infarct area's guidance knowledge fusion are proposed to assess the infarct areas. In general, the larger the infarct area, the higher the possibility of patients with HT after TPA. So IAB separates the local infarct for subsequent assessment of the brain infarct level is more in line with medical diagnostic criterion. In detail, IAB performs local feature encoding based on the ResNet block. Due to the small dataset, the network image encoding and dimensionality reduction ability is weak. By using transfer learning, the ImageNet pre-trained network is used for all three ResNet blocks. Like the

global branch network, the infarct area attention map also passes through a 7x7 convolutional layer with a small receptive field. With small receptive fields, IAB can get more features of the infarct area. Different from traditional ResNet, due to the insufficient number of training samples and to prevent too many network parameters, IAB leverages three layers of ResNet block and combines features with an average pooling layer. To make the numeralization of the infarct area intuitive, we integrate the area guidance knowledge of the infarct area, thus improving the sensitivity of DBSE-Net to the size of the infarct area.

IAB Summarized Advantages: Our newly proposed IAB effectively reduces the dimensionality of the lesion area features through simplified network structure and small receptive field. Through the high-weight infarct attention, the infarct area is enhanced without destroying the image structure. By the infarct area's guidance knowledge fusion mechanism, IAB accurately assesses the infarct area and solves the difficult identification of weak features to a certain extent.

4.4. The fully connection prediction layer

The fully connection prediction layer connects the impact of different single dimensions on the brain status (with or without infarct and compression), which enables global features and local features to impose different weights on HT's prediction (Fig. 3 - Sec4.4). Through HT lesions at two different scales, the layer fuses the local infarct area features and the global brain midline displacement features, thereby achieving higher-precision HT prediction.

5. Experimental Studies and Results

5.1. Data acquisition

We validated the performance of DBSE-Net by 144 intracranial stroke patients, diagnosed by doctors as low HT risk. All prediction results are derived from patients' clinical observations, and all segmentation labels are marked under the guidance of professional brain experts. Each frame image size is 512×512×1 with 40 window level, 80 window width. All patients had a cerebral infarction in the form of trial of org10172 in acute stroke treatment (TOAST)(Adams H P et al., 1993), but TPA was performed in all 144 intracranial stroke patients. The age distribution of TOAST patients was 70.06 as the mean and 11.30 as the standard deviation. All patients have

uneven distribution of infarct areas, and only a small number of patients have large infarct areas. We selected two frames of non-contrast images as a dual-channel image input obtained by the ASPECTS indicator.

5.2. Implementation details

We implement the construction and result testing of neural networks through the Python-based Pytorch library. The experimental environment is Linux (Ubuntu 18.04.1 LTS) desktop computer, equipped with TITAN X (PASCAL) graphics card and 390.48 Nvidia driver. The system memory is 16GB, and the CPU is Intel(R) Core(TM) i7-4790K. The optimizer selected in the experiment is ADAM (lr=0.001, weight_decay=5e-4). To improve experimental credibility, we apply a 5-fold cross-validation method during the experiment. In VW-UNet, we use the standard U-Net model, and the loss weight hyperparameter k of the infarct region is set to 3. In the IAB's infarct area attention mechanism, λ is set to 2 to enhance the local infarct area. To prevent over-fitting, we add a dropout mechanism to the ResNet block the last layer, with a coefficient of 0.7, and the dilated rate in BCAB is set to 2.

5.3. Prediction evaluation index

1) The precision, recall, and accuracy indicators are applied to evaluate the DBSE-Net prediction effect. 2) The kappa statistic is used to measure the agreement of the HT prediction result. 3) The receiver operating characteristic (ROC) curve with the area under ROC curve (AUC) and precision-recall (PR) curve are applied to compare with other scholars' methods. 4) The F_1 Score is proposed to balance precision and recall, which is defined as:

$$F_1 = 2 \cdot \frac{precision \cdot recall}{precision + recall} \tag{3}$$

where precision and recall are defined as:

$$precision = \frac{TP}{TP + FP} \tag{4}$$

$$recall = \frac{TP}{TP + FN} \tag{5}$$

where TP denotes true positive (network prediction is HT, the actual result is HT), FP denotes false positive (network prediction is HT, the actual result is normal), FN denotes false negative (network prediction is normal, the actual result is HT).

5.4. Segmentation evaluation index

1) We first use the most common evaluation indicator: dice coefficient to evaluate the brain region segmentation layer, which is the common indicator to compare with other models. Dice coefficient's result is in the range of [0-1]. The closer the result is to 1, the better the segmentation effect. Dice coefficient is defined as:

$$Dice = \frac{2 \cdot |X \cap Y|}{|X| + |Y|} \times 100\% \tag{6}$$

where X represents the region in the ground truth, Y represents the region in our network segmentation result.

2) Mean intersection over union (mIoU) metric is proposed to averagely evaluate the segmentation status of each category (infarction, left and right brain). The segmentation accuracy range of mIoU is 0-1, where 1 is the perfect segmentation situation(Tam et al., 2020). The mIoU formula is:

$$mIoU = \frac{1}{k+1} \sum_{i=0}^{k} \frac{|X_k \cap Y_k|}{|X_k \cup Y_k|} \tag{7}$$

where k represents the number of categories for segmentation tasks.

3) Kappa statistic is proposed to determine whether the label and the segmentation network output conform to the consistent distribution, the kappa statistic is defined as:

$$kappa = \frac{p_o - p_e}{1 - p_e} \tag{8}$$

where p_o represents the accuracy (number of pixels correctly classified), p_e is defined as:

$$p_e = \frac{P \cdot (TP + FN) + N \cdot (FP + TN)}{(P + N)^2} \tag{9}$$

where P represents the number of positive samples segmented by the network, N represents the number of negative samples segmented by the network. The range of the kappa score is [0,1], and a large kappa statistic indicates better agreement.

Table 1: Horizontal Comparison: The prediction evaluation table points out that DBSE-Net far exceeds traditional neural networks, and can assist doctors in the second HT risk diagnosis.

Method	Precision	Recall	Acc	F_1 Score	Kappa
DenseNet	0.5903	0.7500	0.5263	0.6587	-0.0877
ResNet	0.6623	0.6643	0.5833	0.6615	0.1176
SENet	0.5990	0.6286	0.5132	0.6130	-0.0428
DBSE-Net	**0.7348**	**0.8571**	**0.7193**	**0.7902**	**0.3737**

5.5. Comparison Experiments

Horizontal Comparison Experiment - DBSE-Net: Since no other scholars use non-contrast CT for HT prediction, a horizontal comparison is proposed to evaluate the performance difference between DBSE-Net and common classification networks: ResNet, DenseNet, SENet, which is the winner of the 2017 ILSVR competition. All classification networks use two ASPECTS images as input like DBSE-Net. Table 1 shows the horizontal comparison experiment results of DBSE-Net and common classification neural network models. The results show that traditional neural networks can hardly predict HT from non-contrast CT. Since traditional neural networks mainly classify images based on rich semantic information, but medical image has few semantic information. It is difficult for traditional neural networks to perform well with a relative lack of semantic information and high prediction difficulty. The accuracy rate of about 55% points out that traditional neural networks cannot extract useful brain lesion features, while DBSE-Net can extract sufficient brain structural abnormalities, thereby realizing HT's effective prediction. The 0-0.1 kappa statistics of the traditional neural network also shows that its prediction results are not consistent with the real results. The 0.3737 kappa statistics of DBSE-Net indicate that the predicted results meet the general consistency with the real patient situation. Fig. 5(a) and Fig. 5(b) respectively show the ROC and PR curve from the horizontal comparison experiment, which also proves that DBSE-Net can analyze non-contrast CT to predict HT.

Horizontal Comparison Experiment - ASPECTS Selection Rules: Although we explained the importance of the ASPECTS criterion for feature extraction, there is still a necessity for performance verification from a technical perspective. We perform two frames image offset on each input image selected by the ASPECTS criteria. Based on other experiment con-

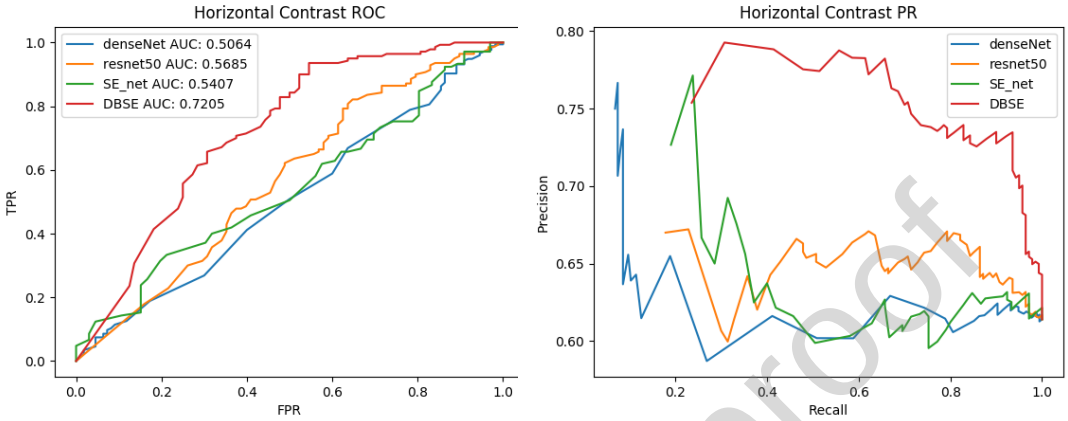

(a) Horizontal Comparison ROC (b) Horizontal Comparison PR

Figure 5: ROC and PR curves show that DBSE-Net has a good performance for HT prediction with non-contrast CT.

Table 2: Horizontal Comparison: The prediction results show that the precise selection of ASPECTS can increase about 5% prediction accuracy.

Method	Acc-Offset	Acc-NonOffset	Improvement
DenseNet	0.5213	0.5263	0.96%
ResNet	0.5428	0.5833	**7.46%**
SENet	0.5156	0.5132	-0.47%
DBSE-Net	**0.6837**	**0.7193**	5.21%

ditions unchanged, test the prediction performance of the baseline network and DBSE-Net.

The prediction results after image offset are shown in Table 2. The small infarct area may not be captured in non-key frames, and the brain structure may be unclear with slight image offset. Table 2 shows that the precise selection of ASPECTS can improve the prediction accuracy to a certain extent.

Horizontal Comparison Experiment - Brain region segmentation layer: We evaluate the brain region segmentation layer's separation effect on the left brain, right brain, and infarct region. Since the segmentation layer determines the accuracy of subsequent feature extraction and area guidance knowledge, the segmentation accuracy needs to be accurately assessed.

Quantitative results in terms of dice coefficient and mIoU are demonstrated in Table 3. As shown in the table, most networks have a good per-

Table 3: Horizontal Comparison: Multiple segmentation evaluations show that VW-UNet has the best segmentation effect and the highest consistency with label data.

	Dice	mIoU	Kappa
DeeplabV3(Chen et al., 2017)	0.9632	0.9609	0.9846
DeeplabV3+(Chen et al., 2018)	0.9554	0.9508	0.9770
PSPNet(Zhao et al., 2017)	0.9602	0.9575	0.9822
UNet(Ronneberger et al., 2015)	0.9657	0.9634	0.9857
VW-UNet	**0.9706**	**0.9644**	**0.9876**

formance on the brain segmentation, and VW-UNet is the most prominent network. Simultaneously, the ultra-high kappa statistic also points out that the segmentation network result is remarkably consistent with the original label.

The segmentation results from different networks are shown in Fig. 6. From sample 1 and sample 2, VW-UNet is the network with the highest fit to the infarct area among all networks. From sample 3, DeeplabV3 and UNet mis-segments brain tissue: sylvian fissure, not the infarct area while VW-UNet does not mis-segment. From sample 4, only VW-UNet successfully segmented the infarct area. From sample 5, for multi-region infarct region segmentation, UNet successfully segmented one of the infarct regions, but only VW-UNet successfully segmented all infarct regions. From all the samples, UNet and VW-UNet have the best segmentation effect on brain regions. However, VW-UNet has a better segmentation effect on the infarct area, but has a small part of brain tissue region mis-segmentations.

Ablation Comparison Experiment - Brain region segmentation layer: To test the effectiveness of VW-UNet in prediction task, we choose the traditional segmentation network to replace VW-UNet to implement ablation experiments (Table 4). In Table 4, VW-UNet has the best adaptability to DBSE-Net. Different networks' prediction effects have little difference in prediction tasks. Although UNet has the highest recall value and PSPNet has the highest precision value, VW-UNet has the best AUC and accuracy for the prediction task. VW-UNet increases the weight of the infarct area and improves the accuracy of the key information about the infarct area, which is more in line with infarct assessment. Fig. 7(a) and Fig. 7(b) respectively show the ROC and PR curve about the brain region segmentation layer ablation experiment. Through ROC and PR curves, the effectiveness of VW-UNet can be visually demonstrated.

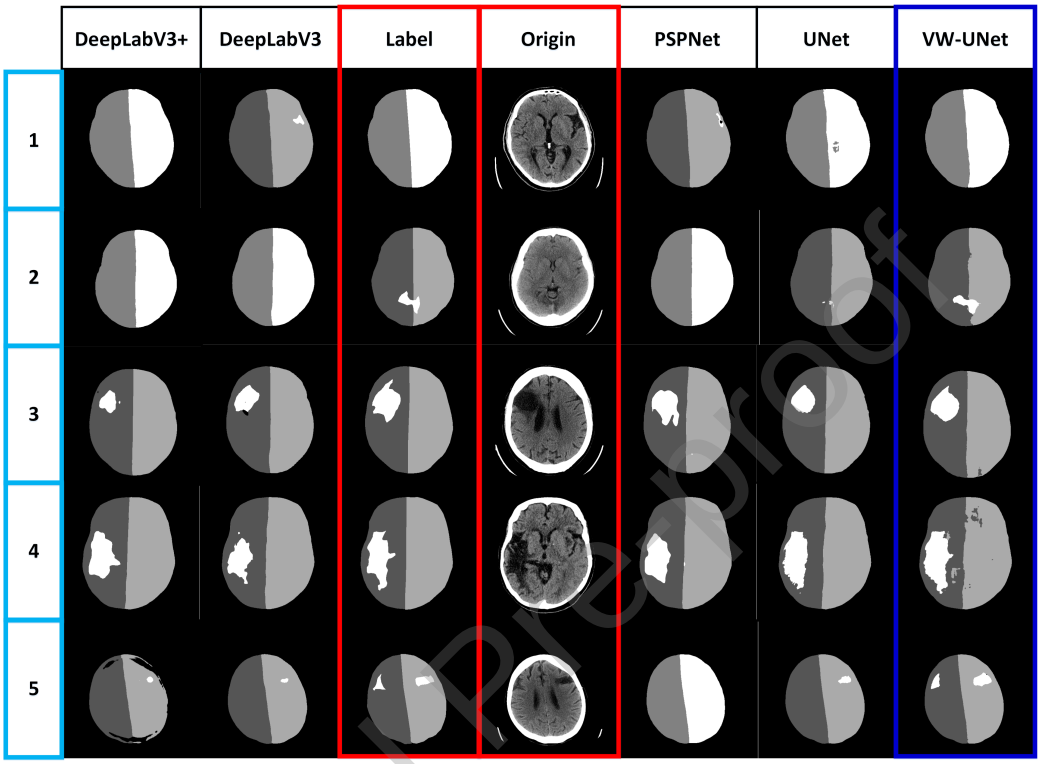

Figure 6: Comparison of segmentation effects of brain region segmentation layer: The segmentation output results show that VW-UNet focuses more on the infarct area and performs better under complex infarct shapes.

Table 4: Ablation Comparison: Replacing VW-UNet with traditional segmentation networks. The effectiveness of VW-UNet is verified by different networks' prediction results. Among all networks, the most suitable brain region segmentation layer for DBSE-Net is VW-UNet.

Seg Layer	Precision	Recall	Acc	F_1 Score	Kappa
PSPNet	**0.7593**	0.7929	0.7061	0.7634	0.3667
DeepLabV3	0.7209	0.8429	0.7018	0.7764	0.3362
DeepLabV3P	0.7201	0.8214	0.6930	0.7665	0.3230
UNet	0.7199	**0.8857**	0.7105	0.7892	0.3363
VW-UNet	0.7348	0.8571	**0.7193**	**0.7902**	**0.3737**

Ablation Comparison Experiment - Feature Encoding layer: We use the traditional prediction neural network to test the necessity of the dual-branch encoding layer. As shown in Table 5, the DBSE-Net encoding

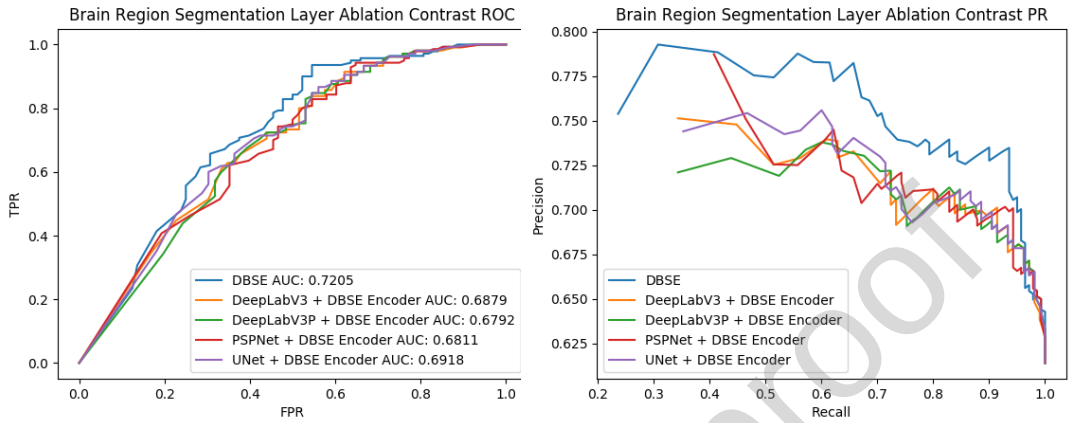

(a)Ablation Comparison ROC (b) Ablation Comparison PR

Figure 7: ROC and PR curves show that VW-UNet is the most suitable substructure for DBSE-Net.

Table 5: Ablation Comparison: Replace dual-branch feature encoding layer with traditional classification encoder networks. Verify the dual-branch feature encoding layer's effectiveness based on the prediction effect of the overall network. The results show that the IAB+BCAB encoding structure is most suitable for DBSE-Net.

Encoder	Precision	Recall	Acc	F_1 Score	Kappa
DenseNet	0.6337	0.8214	0.5877	0.7008	0.0343
SENet	0.6906	0.6571	0.5789	0.6340	0.1063
ResNet	0.7271	0.7714	0.6798	0.7475	0.3101
IAB+BCAB	**0.7348**	**0.8571**	**0.7193**	**0.7902**	**0.3737**

layer is compared with DenseNet, ResNet and SEnet. In this experiment, the input of the traditional neural network is a four-channel ASPECTS non-contrast CT image. The four channel image is the superposition of the brain region segmentation layer output and the DBSE-Net original input image. As shown in Table 5, DenseNet and SEnet are not suitable for the feature encoding task of HT prediction. Compared with Table 1, ResNet uses a pre-segmentation network to greatly improve the prediction effect. However, the joint feature encoding structure of IAB+BCAB exceeds the single encoding structure of ResNet in all aspects, and becomes the most suitable feature encoding structure for DBSE-Net. To clearly describe the differences between the various networks, we also used the ROC and PR curves in Fig. 8(a) and

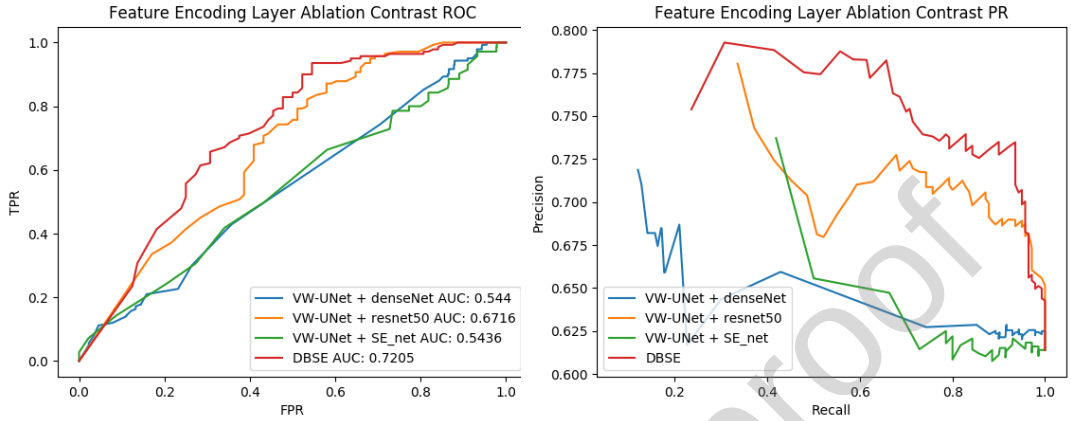

(a) Ablation Comparison ROC (b) Ablation Comparison PR

Figure 8: ROC and PR show that the IAB+BCAB encoder is most suitable for the DBSE-Net structure.

Table 6: Ablation Comparison: DBSE-Net is compared with the effect of retaining only a single branch. The experimental results show that the single branch is not suitable for HT prediction mode, and only the dual branch of IAB+BCAB can achieve accurate HT prediction.

DBSE		Precision	Recall	Acc	F_1	Kappa
BCAB	IAB					
✓		0.6947	0.7143	0.6316	0.7038	0.2162
	✓	0.6598	0.7286	0.6001	0.6914	0.1290
✓	✓	0.7348	0.8571	0.7193	0.7902	0.3737

Fig. 8(b).

Ablation Comparison Experiment - IAB & BCAB: To test the effectiveness of each branch, we apply an ablation experiment to detect local branch and global branch separately, which is shown in Tabel 6. The table shows that the BCAB global branch has a significant improvement in the prediction of HT. Due to the introduction of area guidance knowledge and the guidance of pre-segmented regions, the BCAB global branch focuses on distinguishing the infarct area and whether the brain area has a midline displacement phenomenon. On the contrary, the improvement of the IAB local branch is limited. Compared with traditional neural networks, the assistance of area guidance knowledge and network structure optimization make local

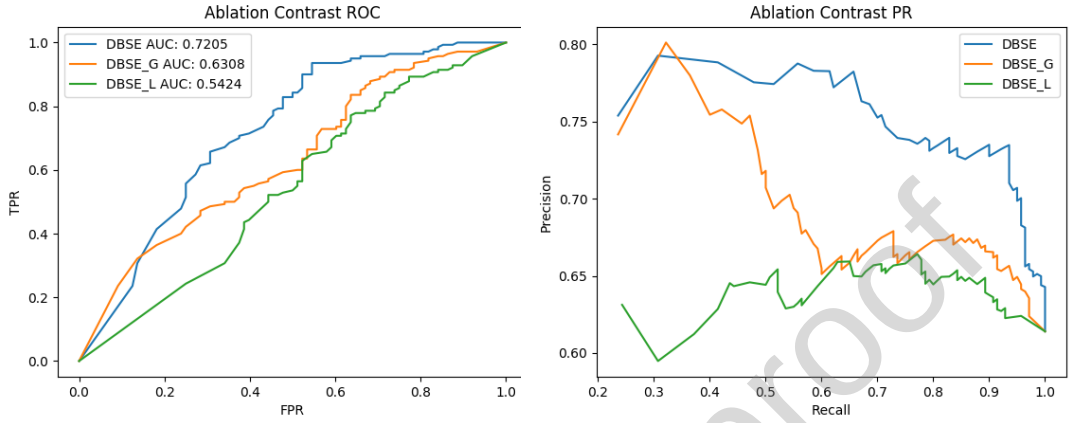

(a) Ablation Comparison ROC (b) Ablation Comparison PR

Figure 9: The ablation comparison curve between DBSE-Net and its respective branches. DBSE_G means to reserve the BCAB branch (Global), DBSE_L means to reserve the IAB branch (Local). ROC and PR results show that only the dual-branch combination of IAB+BCAB can achieve accurate HT prediction.

branches still have HT prediction ability. It can be seen from kappa statistics that BCAB and IAB branches have a poor correlation with HT's prediction results. However, the DBSE-Net combines the BCAB branch and the IAB branch, making the two branch networks complementary, thereby achieving HT prediction on non-contrast CT. From the perspective of DBSE-Net's high recall index, DBSE-Net is inclined to conservative HT treatment, which is also in line with the medical community's current status to avoid high HT risks. For a clear description of the DBSE-Net's each branch performance, the ROC curve and the PR curve are presented in Fig. 9(a) and Fig. 9(b).

To describe the effectiveness of the network structure and explain the intermediate feature information of the DBSE-Net, the intermediate feature map is presented in Fig. 10. The feature results of L_Layer1 and L_Layer2 can clearly show that the global branch focuses on the infarct location, the area of the infarct, and the boundary between the left and right brains. According to the segmentation results and the performance of L_Layer1, the local branch's pre-feature extraction entirely depends on the accuracy of the segmentation network. From the performance of G_Layer1 and G_Layer2, the local branch pays more attention to the infarct details and the brain tissue features (brain compression).

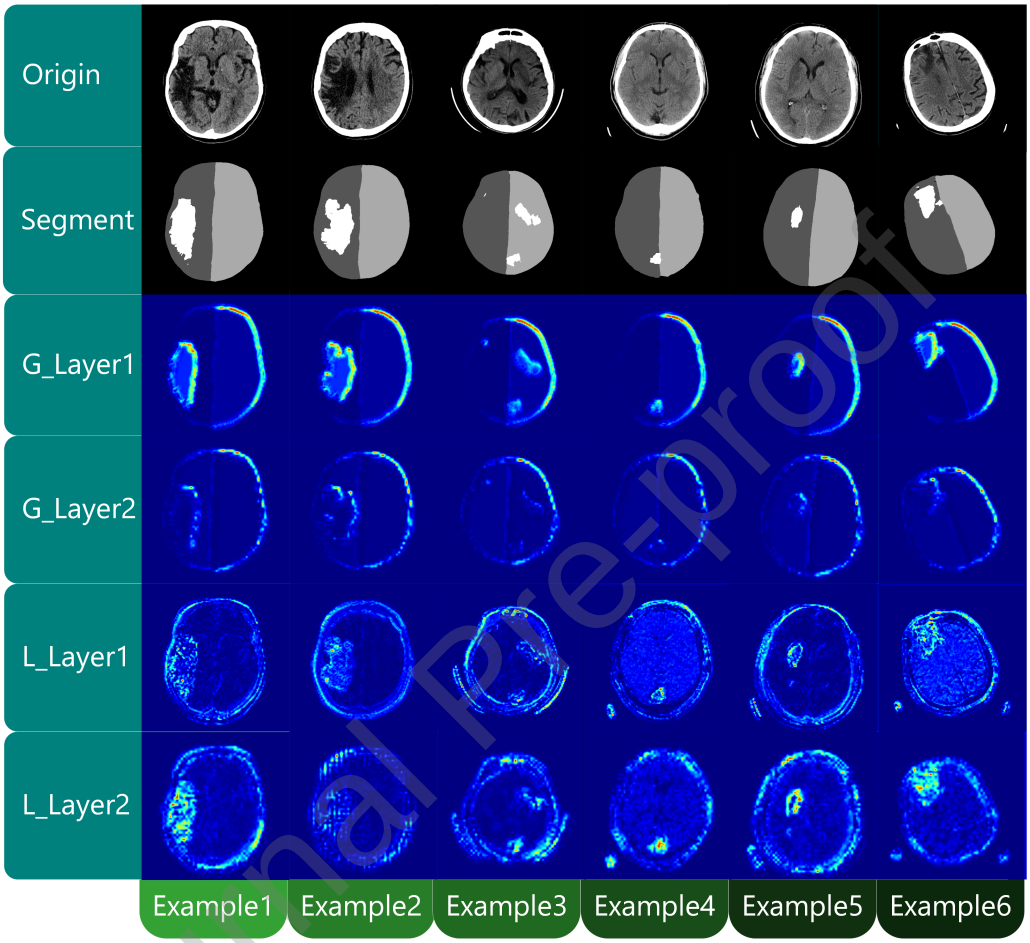

Figure 10: DBSE-Net's dual-branch middle layer output heat map. G_Layer means the BCAB branch layer, L_Layer means the IAB branch layer. The heat map shows that each layer of the DBSE-Net effectively pays attention to the infarct area and the global brain compression.

6. Discussion and conclusion

In this paper, our main contribution is that, for the first time, we achieve HT prediction based on non-contrast CT, which is difficult and of great medical significance. The non-contrast CT-based HT prediction method can effectively reduce the possibility of the patient being injured by the perfusion agent and save the economic cost, labor cost, and time cost. Our framework is built on a dual-branch feature separation and enhanced neural network

(DBSE-Net) to achieve the accurate HT prediction. The dual branch separation and enhancement mechanism in DBSE-Net effectively extract the multi-category and multi-scale lesion features. Simultaneously, DBSE-Net solves the poor relationship problem through adaptive feature encoding and introduction of guidance knowledge. Based on the redundant information removal of the ASPECTS keyframe selection layer, DBSE-Net enhances the keyframe lesion features. Relying on the adaptive feature encoding structure (BCAB and IAB) and VW-UNet which pays more attention to the infarct area, DBSE-Net effectively extracts weak lesion features. DBSE-Net solves the problems of poor relationship and weak feature extraction, thus realizing accurate HT prediction. The prediction accuracy (0.72 to 0.55±0.03) and kappa statistics (0.37 to 0.02±0.09) far exceeding that of the conventional classification network demonstrate the effectiveness of DBSE-Net.

In summary, we use 288 non-contrast CT images from 144 patients to achieve an accurate preliminary prediction of HT. Previous research works do not choose HT prediction based on non-contrast CT, which is realized by our study. Through our non-contrast CT prediction method, a large number of high-risk HT patients will be rescued. We hope that in the future, non-contrast CT prediction algorithms with higher accuracy and better prediction effect can be proposed to save patients' lives.

Declaration of interests

The authors declare that they have no known competing financial interests or personal relationships that could have appeared to influence the work reported in this paper.

References

Adams H P, Bendixen B H, Kappelle L J, Biller J, Love B B, Gordon D L, Marsh E E, 1993. Classification of subtype of acute ischemic stroke. Definitions for use in a multicenter clinical trial. TOAST. Trial of Org 10172 in Acute Stroke Treatment. Stroke 24, 35–41. URL: https://www.ahajournals.org/doi/abs/10.1161/01.str.24.1.35, doi:10.1161/01.STR.24.1.35. publisher: American Heart Association.

Aviv, R.I., d'Esterre, C.D., Murphy, B.D., Hopyan, J.J., Buck, B., Mallia, G., Li, V., Zhang, L., Symons, S.P., Lee, T.Y., 2009. Hemorrhagic Trans-

formation of Ischemic Stroke: Prediction with CT Perfusion. Radiology 250, 867–877. URL: https://pubs.rsna.org/doi/full/10.1148/radiol.2503080257, doi:10.1148/radiol.2503080257. publisher: Radiological Society of North America.

Bang, O.Y., Buck, B.H., Saver, J.L., Alger, J.R., Yoon, S.R., Starkman, S., Ovbiagele, B., Kim, D., Ali, L.K., Sanossian, N., Jahan, R., Duckwiler, G.R., Viñuela, F., Salamon, N., Villablanca, J.P., Liebeskind, D.S., 2007. Prediction of hemorrhagic transformation after recanalization therapy using T2*-permeability magnetic resonance imaging. Annals of Neurology 62, 170–176. URL: https://onlinelibrary.wiley.com/doi/abs/10.1002/ana.21174, doi:10.1002/ana.21174. _eprint: https://onlinelibrary.wiley.com/doi/pdf/10.1002/ana.21174.

Barbier, E.L., Lamalle, L., Décorps, M., 2001. Methodology of brain perfusion imaging. Journal of Magnetic Resonance Imaging: An Official Journal of the International Society for Magnetic Resonance in Medicine 13, 496–520.

Bouts, M.J., Tiebosch, I.A., Rudrapatna, U.S., van der Toorn, A., Wu, O., Dijkhuizen, R.M., 2017. Prediction of hemorrhagic transformation after experimental ischemic stroke using MRI-based algorithms. Journal of Cerebral Blood Flow & Metabolism 37, 3065–3076. URL: https://doi.org/10.1177/0271678X16683692, doi:10.1177/0271678X16683692. publisher: SAGE Publications Ltd STM.

Broocks, G., Flottmann, F., Scheibel, A., Aigner, A., Faizy, T.D., Hanning, U., Leischner, H., Broocks, S.I., Fiehler, J., Gellissen, S., et al., 2018. Quantitative lesion water uptake in acute stroke computed tomography is a predictor of malignant infarction. Stroke 49, 1906–1912.

C, O., Y, S., D, D., S, C., R, M., G, R., D, F., C, M., 2002. DWI prediction of symptomatic hemorrhagic transformation in acute MCA infarct. Journal of Neuroradiology = Journal de Neuroradiologie 29, 6–13. URL: https://europepmc.org/article/med/11984472.

Chen, L.C., Papandreou, G., Schroff, F., Adam, H., 2017. Rethinking atrous convolution for semantic image segmentation. arXiv preprint arXiv:1706.05587 .

Chen, L.C., Zhu, Y., Papandreou, G., Schroff, F., Adam, H., 2018. Encoder-decoder with atrous separable convolution for semantic image segmentation, in: Proceedings of the European conference on computer vision (ECCV), pp. 801–818.

Hu, J., Shen, L., Sun, G., 2018. Squeeze-and-excitation networks, in: Proceedings of the IEEE conference on computer vision and pattern recognition, pp. 7132–7141.

Huang, G., Liu, Z., Van Der Maaten, L., Weinberger, K.Q., 2017. Densely connected convolutional networks, in: Proceedings of the IEEE conference on computer vision and pattern recognition, pp. 4700–4708.

Hunter, G.J., Hamberg, L.M., Ponzo, J.A., Huang-Hellinger, F.R., Morris, P.P., Rabinov, J., Farkas, J., Lev, M.H., Schaefer, P.W., Ogilvy, C.S., et al., 1998. Assessment of cerebral perfusion and arterial anatomy in hyperacute stroke with three-dimensional functional ct: early clinical results. American Journal of Neuroradiology 19, 29–37.

Hutchinson, M.L., Beslow, L.A., 2019. Hemorrhagic Transformation of Arterial Ischemic and Venous Stroke in Children. Pediatric Neurology 95, 26–33. URL: http://www.sciencedirect.com/science/article/pii/S0887899418313006, doi:10.1016/j.pediatrneurol.2019.01.023.

Kim, E.Y., Na, D.G., Kim, S.S., Lee, K.H., Ryoo, J.W., Kim, H.K., 2005. Prediction of Hemorrhagic Transformation in Acute Ischemic Stroke: Role of Diffusion-Weighted Imaging and Early Parenchymal Enhancement. American Journal of Neuroradiology 26, 1050–1055. URL: http://www.ajnr.org/content/26/5/1050. publisher: American Journal of Neuroradiology Section: BRAIN.

Knight, R.A., Barker, P.B., Fagan, S.C., Li, Y., Jacobs, M.A., Welch, K.M.A., 1998. Prediction of impending hemorrhagic transformation in ischemic stroke using magnetic resonance imaging in rats. Stroke 29, 144–151. URL: https://jhu.pure.elsevier.com/en/publications/prediction-of-impending-hemorrhagic-transformation-in-ischemic-st-4, doi:10.1161/01.STR.29.1.144. publisher: Lippincott Williams and Wilkins.

Larrue, V., von Kummer, R., del Zoppo, G., Bluhmki, E., 1997. Hemorrhagic transformation in acute ischemic stroke: potential contributing factors in the european cooperative acute stroke study. Stroke 28, 957–960.

Lin, K., Kazmi, K.S., Law, M., Babb, J., Peccerelli, N., Pramanik, B.K., 2007. Measuring Elevated Microvascular Permeability and Predicting Hemorrhagic Transformation in Acute Ischemic Stroke Using First-Pass Dynamic Perfusion CT Imaging. American Journal of Neuroradiology 28, 1292–1298. URL: http://www.ajnr.org/content/28/7/1292, doi:10.3174/ajnr.A0539. publisher: American Journal of Neuroradiology Section: BRAIN.

Mozaffarian, D., Benjamin, E.J., Go, A.S., Arnett, D.K., Blaha, M.J., Cushman, M., De Ferranti, S., Després, J.P., Fullerton, H.J., Howard, V.J., et al., 2015. Executive summary: heart disease and stroke statistics—2015 update: a report from the american heart association. Circulation 131, 434–441.

Neumann-Haefelin C., Brinker G., Uhlenküken U., Pillekamp F., Hossmann K-A., Hoehn M., 2002. Prediction of Hemorrhagic Transformation After Thrombolytic Therapy of Clot Embolism. Stroke 33, 1392–1398. URL: https://www.ahajournals.org/doi/full/10.1161/01.str.0000014619.59851.65, doi:10.1161/01.STR.0000014619.59851.65. publisher: American Heart Association.

of Neurological Disorders, N.I., rt PA Stroke Study Group, S., 1995. Tissue plasminogen activator for acute ischemic stroke. New England Journal of Medicine 333, 1581–1588.

Pexman, J.W., Barber, P.A., Hill, M.D., Sevick, R.J., Demchuk, A.M., Hudon, M.E., Hu, W.Y., Buchan, A.M., 2001. Use of the alberta stroke program early ct score (aspects) for assessing ct scans in patients with acute stroke. American Journal of Neuroradiology 22, 1534–1542.

Qiu, W., Kuang, H., Teleg, E., Ospel, J.M., Sohn, S.I., Almekhlafi, M., Goyal, M., Hill, M.D., Demchuk, A.M., Menon, B.K., 2020. Machine learning for detecting early infarction in acute stroke with non–contrast-enhanced ct. Radiology 294, 638–644.

Ronneberger, O., Fischer, P., Brox, T., 2015. U-net: Convolutional networks for biomedical image segmentation, in: International Conference on Medical image computing and computer-assisted intervention, Springer. pp. 234–241.

Sussman, E.S., Connolly Jr, E.S., 2013. Hemorrhagic transformation: a review of the rate of hemorrhage in the major clinical trials of acute ischemic stroke. Frontiers in neurology 4, 69.

Szegedy, C., Ioffe, S., Vanhoucke, V., Alemi, A., 2016. Inception-v4, inception-resnet and the impact of residual connections on learning. arXiv preprint arXiv:1602.07261 .

Tam, C.M., Zhang, D., Chen, B., Peters, T., Li, S., 2020. Holistic multitask regression network for multiapplication shape regression segmentation. Medical Image Analysis 65, 101783.

Wang, Q., Reps, J.M., Kostka, K.F., Ryan, P.B., Zou, Y., Voss, E.A., Rijnbeek, P.R., Chen, R., Rao, G.A., Stewart, H.M., Williams, A.E., Williams, R.D., Zandt, M.V., Falconer, T., Fernandez-Chas, M., Vashisht, R., Pfohl, S.R., Shah, N.H., Kasthurirathne, S.N., You, S.C., Jiang, Q., Reich, C., Zhou, Y., 2020. Development and validation of a prognostic model predicting symptomatic hemorrhagic transformation in acute ischemic stroke at scale in the OHDSI network. PLOS ONE 15, e0226718. URL: https://journals.plos.org/plosone/article?id=10.1371/journal.pone.0226718, doi:10.1371/journal.pone.0226718. publisher: Public Library of Science.

Wiley, G., 2008. The new economics of contrast. https://www.radiologybusiness.com/topics/business-intelligence/new-economics-contrast. Accessed September 02, 2008.

Xu, C., Zhang, D., Chong, J., Chen, B., Li, S., 2021. Synthesis of gadolinium-enhanced liver tumors on nonenhanced liver mr images using pixel-level graph reinforcement learning. Medical Image Analysis 69, 101976.

Yassi Nawaf, Parsons Mark W., Christensen Søren, Sharma Gagan, Bivard Andrew, Donnan Geoffrey A., Levi Christopher R., Desmond Patricia M., Davis Stephen M., Campbell Bruce C.V., 2013. Prediction of Poststroke